IMMUNOTHERAPY

Targeting monoamine oxidase A for T cell–based cancer immunotherapy

Xi Wang[1], Bo Li[1], Yu Jeong Kim[1], Yu-Chen Wang[1], Zhe Li[1], Jiaji Yu[1], Samuel Zeng[1], Xiaoya Ma[1], In Young Choi[1], Stefano Di Biase[1], Drake J. Smith[1], Yang Zhou[1], Yan-Ruide Li[1], Feiyang Ma[2], Jie Huang[1], Nicole Clarke[1], Angela To[1], Laura Gong[1], Alexander T. Pham[1], Heesung Moon[1], Matteo Pellegrini[2,3], Lili Yang[1,4,5,6]*

Monoamine oxidase A (MAO-A) is an enzyme best known for its function in the brain, where it breaks down neurotransmitters and thereby influences mood and behavior. Small-molecule MAO inhibitors (MAOIs) have been developed and are clinically used for treating depression and other neurological disorders. However, the involvement of MAO-A in antitumor immunity has not been reported. Here, we observed induction of the *Maoa* gene in tumor-infiltrating immune cells. *Maoa* knockout mice exhibited enhanced antitumor T cell immunity and suppressed tumor growth. MAOI treatment significantly suppressed tumor growth in preclinical mouse syngeneic and human xenograft tumor models in a T cell–dependent manner. Combining MAOI and anti–PD-1 treatments generated synergistic tumor suppression effects. Clinical data correlation studies associated intratumoral *MAOA* expression with T cell dysfunction and decreased patient survival in a broad range of cancers. We further demonstrated that MAO-A restrains antitumor T cell immunity through controlling intratumoral T cell autocrine serotonin signaling. Together, these data identify MAO-A as an immune checkpoint and support repurposing MAOI antidepressants for cancer immunotherapy.

INTRODUCTION

CD8 cytotoxic T cells are potent immune cells capable of recognizing and eradicating malignant cells; these immune cells are therefore attractive therapeutic targets for treating cancer (*1*–*3*). However, the antitumor responses of CD8 T cells can be severely restrained by negative-regulator (immune checkpoint) pathways that are particularly prevalent in the tumor immunosuppressive environment (*4*). To release this suppression and harness the antitumor potential of CD8 T cells, several immune checkpoint blockade (ICB) therapies have been developed over the past decade (*5*, *6*). Blockade of the cytotoxic T lymphocyte–associated protein 4 (CTLA-4) and programmed cell death protein 1 (PD-1)/programmed cell death 1 ligand 1 (PD-L1) inhibitory pathways have achieved remarkable clinical responses and revolutionized the treatment of many cancers; so far, the U.S. Food and Drug Administration (FDA) has approved these two ICB therapies for treating more than 10 different malignancies (*5*, *6*). Despite these impressive successes, only a fraction of patients with cancer respond to CTLA-4 and PD-1/PD-L1 blockade therapies, and most responders suffer tumor recurrence due to the development of tumor immune evasion (*7*). These limitations of existing ICB therapies are thought to be largely caused by the presence of multiple immune checkpoint pathways, as well as the different roles of individual immune checkpoint pathways in regulating specific cancer types and disease stages (*7*). Thus, the identification of new immune checkpoints and the development of new combination treatments are a major focus of current cancer immunotherapy studies.

Monoamine oxidase A (MAO-A) is an enzyme that catalyzes the degradation of biogenic and dietary monoamines (*8*, *9*). MAO-A is located on the outer membrane of mitochondria and, in humans, is encoded by the X-linked *MAOA* gene. MAO-A is best known for its function in the brain, where it regulates the homeostasis of key monoamine neuronal transmitters including serotonin, dopamine, epinephrine, and norepinephrine and thereby influences human mood and behavior (*8*, *9*). Complete MAO-A deficiency in humans caused by a mutation of the *MAOA* gene leads to an excess of monoamine neuronal transmitters in the brain and results in Brunner syndrome, which is characterized by problematic impulsive behaviors and mood swings (*10*). Genetic association studies also identified several *MAOA* gene variants linked to altered MAO-A enzyme expression levels: Low-activity forms of the *MAOA* gene are associated with aggression and hyperactivity disorders, whereas high-activity forms are associated with depression disorders (*11*, *12*). Because of its link with aggressive and even violent behavior in men, a low-activity variant of the *MAOA* gene, *MAOA-L*, has previously received broad publicity and is popularly referred to as the "warrior gene" (*13*). On the other hand, small-molecule MAO inhibitors (MAOIs) have been developed and are clinically used for treating depression symptoms (*14*). However, MAO-A's functions outside of the brain are largely unexplored. In particular, the involvement of MAO-A in antitumor immunity is unknown. Here, we investigated the role of MAO-A in regulating CD8 T cell antitumor immunity and evaluated the possibility of repurposing MAOIs for cancer immunotherapy using knockout (KO) and transgenic mice, preclinical mouse syngeneic and human xenograft tumor models, and clinical data correlation studies.

[1]Department of Microbiology, Immunology and Molecular Genetics, University of California, Los Angeles, CA 90095, USA. [2]Department of Molecular, Cell and Developmental Biology, University of California, Los Angeles, CA 90095, USA. [3]Institute for Genomics and Proteomics, University of California, Los Angeles, CA 90095, USA. [4]Molecular Biology Institute, University of California, Los Angeles, CA 90095, USA. [5]Eli and Edythe Broad Center of Regenerative Medicine and Stem Cell Research, University of California, Los Angeles, CA 90095, USA. [6]Jonsson Comprehensive Cancer Center, the David Geffen School of Medicine, University of California, Los Angeles, CA 90095, USA.
*Corresponding author. Email: liliyang@ucla.edu

RESULTS

MAO-A deficiency enhances CD8 T cell antitumor immunity

To search for new drug targets regulating antitumor immunity, we grew B16–ovalbumin (OVA) melanoma solid tumors in C57BL/6J mice, isolated tumor-infiltrating immune cells (TIIs), and evaluated TII gene expression profiles using quantitative reverse transcription polymerase chain reaction (RT-PCR). Immune cells isolated from the spleen of tumor-bearing and tumor-free mice were included as controls. In addition to the classical immune regulatory genes, we detected significant changes in the expression of a group of genes typically classified as neuronal regulatory genes. In particular, we detected the induction of a *Maoa* gene in TIIs (Fig. 1A), suggesting that, along with its known function in the brain as a regulator of neuronal activity (*8*), it might also function in the tumor as a regulator of antitumor reactivity. We were especially interested to study whether MAO-A might regulate CD8 cytotoxic T cells, which play a critical role in immune response against cancer.

To test this, we began by studying MAO-A–deficient mice that carry a hypomorphic *Maoa* mutant (*15*). Although a degree of *Maoa* expression leakage in the brain was previously reported in these mice (*15*), analysis of their immune system showed a nearly complete ablation of *Maoa* mRNA and protein expression in the major immune organs including thymus and spleen (fig. S1, A and B). Since we focused on studying immune cells, here, we refer to these mice as *Maoa*-KO mice. *Maoa*-KO mice showed normal T cell development in the thymus and contained normal numbers of T cells in the periphery, compared with the wild-type control mice (*Maoa*-WT mice) (fig. S1, C to H). Before tumor challenge, these T cells displayed a typical naïve phenotype ($CD25^{lo}CD69^{lo}CD44^{lo}CD62L^{hi}$; fig. S1I). When challenged with tumors, compared with *Maoa*-WT mice, *Maoa*-KO mice exhibited significantly suppressed tumor growth in two syngeneic mouse tumor models, the MC38 colon cancer model and the B16-OVA melanoma model (Fig. 1, B to D). Flow cytometry analysis detected similar levels of tumor-infiltrating CD8 T cells in *Maoa*-KO and *Maoa*-WT mice (fig. S2A). However, in *Maoa*-KO mice, these tumor-infiltrating T cells displayed an enhanced effector phenotype: They produced higher levels of effector cytokines and cytotoxic molecules [i.e., interferon-γ (IFN-γ) and

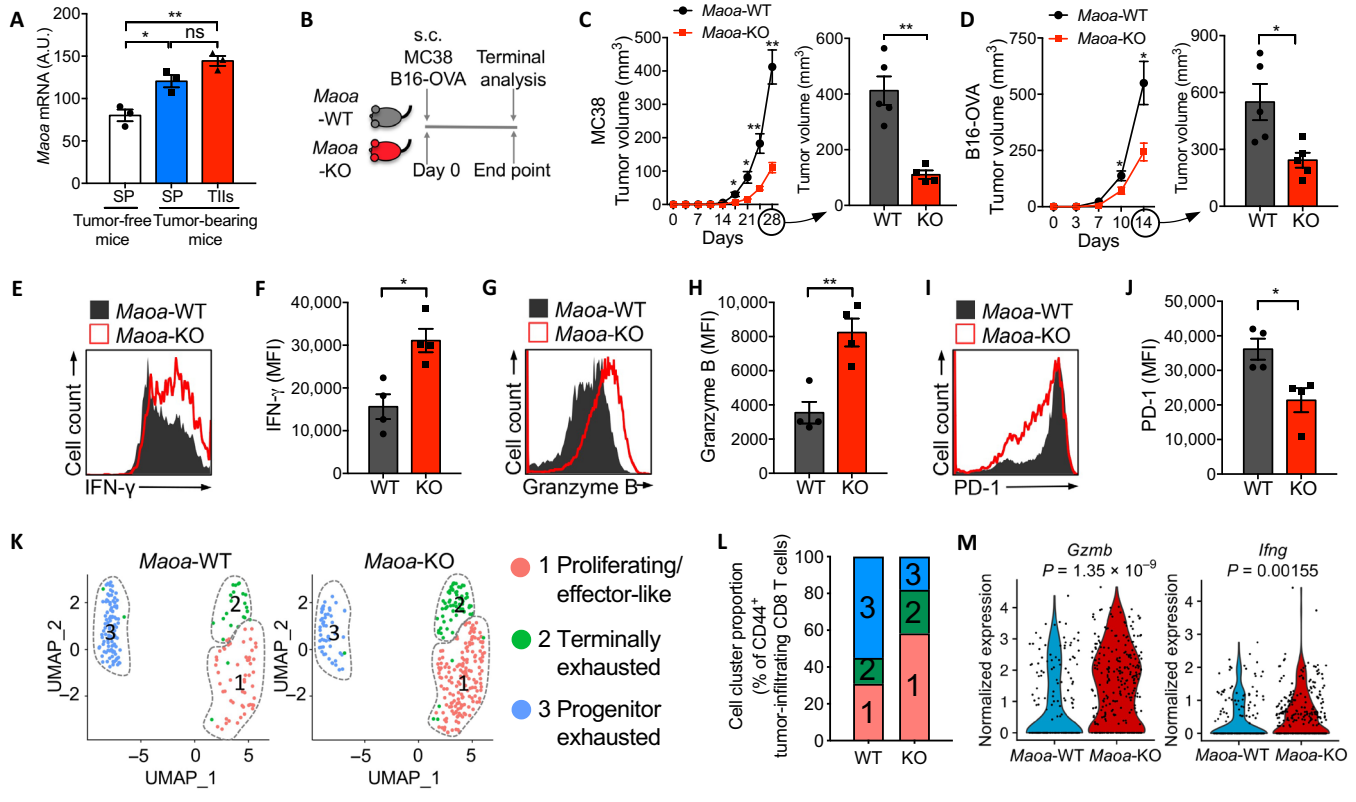

Fig. 1. MAO-A–deficient mice show suppressed tumor growth and enhanced CD8 T cell antitumor immunity. (**A**) qPCR analyses of *Maoa* mRNA expression in TIIs isolated from day 14 B16-OVA melanoma tumors grown in wild-type B6 mice ($n = 3$). Spleen (SP) cells collected from the tumor-bearing and tumor-free B6 mice were included as controls. A.U., artificial unit. (**B** to **D**) Syngeneic tumor growth in *Maoa*-WT and *Maoa*-KO mice. s.c., subcutaneous. (B) Experimental design. (C) MC38 colon cancer tumor growth ($n = 4$ and 5). (D) B16-OVA melanoma tumor growth ($n = 5$). (**E** to **J**) Flow cytometry analysis of tumor-infiltrating CD8 T cells isolated from day 14 B16-OVA tumors grown in *Maoa*-WT and *Maoa*-KO mice ($n = 4$). FACS plots and quantifications are presented, showing the measurements of intracellular IFN-γ (E and F) and Granzyme B (G and H) production, as well as cell surface PD-1 expression (I and J). MFI, mean fluorescence intensity. (**K** to **M**) scRNA-seq analysis of antigen-experienced ($CD44^+$) tumor-infiltrating CD8 T cells isolated from day 14 B16-OVA tumors grown in *Maoa*-WT and *Maoa*-KO mice (10 tumors were combined for each group). (K) UMAP plots showing the formation of three major cell clusters. Each dot represents a single cell and is colored according to its cell cluster assignment. Gene signature profiling analysis identified cluster 1 cells to be proliferating/effector-like CD8 T cells, cluster 2 cells to be terminally exhausted CD8 T cells, and cluster 3 cells to be progenitor exhausted CD8 T cells. (L) Bar graphs showing the cell cluster proportions. (M) Violin plots showing the expression distribution of *Gzmb* and *Ifng* genes. Each dot represents an individual cell. Representative of one (K to M), two (A), and three (B to J) experiments. Data are presented as the means ± SEM. ns, not significant; $^*P < 0.05$ and $^{**}P < 0.01$ by one-way ANOVA (A) or by Student's *t* test (C, D, F, H, and J). *P* values of violin plots (M) were determined by Wilcoxon rank sum test.

Granzyme B; Fig. 1, E to H], and they expressed lower levels of T cell exhaustion markers (i.e., PD-1; Fig. 1, I and J).

To further investigate how MAO-A deficiency may affect the tumor-infiltrating CD8 T cell compartment, we isolated TIIs from tumor-bearing *Maoa*-WT and *Maoa*-KO mice and performed a single-cell RNA sequencing (scRNA-seq) study. Uniform Manifold Approximation and Projection (UMAP) analysis of antigen-experienced ($CD44^+$) tumor-infiltrating CD8 T cells revealed the formation of three major cell clusters (Fig. 1K); signature gene profiling study (fig. S2, B and C) and gene set enrichment analysis (GSEA; fig. S2, D to F) identified cluster 1 cells as proliferating/effector-like CD8 T cells, cluster 2 cells as terminally exhausted CD8 T cells, and cluster 3 cells as progenitor-exhausted CD8 T cells (*16*). Compared with their wild-type counterparts, *Maoa*-KO tumor-infiltrating CD8 T cells were enriched for proliferating/effector-like (cluster 1) cells while decreased for exhausted (clusters 2 and 3), especially the progenitor-exhausted (cluster 3) cells (Fig. 1, K and L). Single-gene expression analysis also showed an overall enhanced expression of genes associated with cytotoxic T cell effector function (i.e., *Gzmb* and *Ifng*; Fig. 1M) and genes associated with mitochondrial function that is a notable factor in T cell effector function (i.e., mitochondrial electron transport chain genes; fig. S3) (*17*), in tumor-infiltrating CD8 T cells isolated from *Maoa*-KO mice. Collectively, these scRNA-seq results suggest a possible role of MAO-A in regulating the generation/maintenance of active effector-like antitumor CD8 T cells. Together, these in vivo studies using MAO-A–deficient mice indicate that MAO-A is involved in regulating antitumor immunity, especially in regulating CD8 T cell antitumor effector functions.

MAO-A directly regulates CD8 T cell antitumor immunity

In our *Maoa*-KO mice tumor challenge study, MAO-A deficiency affected both immune and nonimmune cells. To determine whether MAO-A directly or indirectly regulates immune cells, we performed a pair of two-way bone marrow (BM) transfer experiments: In one experiment, we confined MAO-A deficiency comparison to immune cells by reconstituting CD45.1 wild-type recipient mice with BM cells from either CD45.2 *Maoa*-WT or *Maoa*-KO donor mice, followed by B16-OVA tumor challenge; in another experiment, we confined MAO-A deficiency comparison to nonimmune cells by reconstituting either CD45.2 *Maoa*-WT or *Maoa*-KO recipient mice with BM cells from CD45.1 wild-type donor mice, followed by B16-OVA tumor challenge (Fig. 2A). Successful reconstitution of immune cells, particularly T cells, was confirmed in both experiments (fig. S4, A to D). Suppressed tumor growth was observed only when MAO-A deficiency was confined to the immune cells, indicating that MAO-A affects tumor growth via directly regulating immune cell antitumor reactivity (Fig. 2, B and C).

To further study whether MAO-A directly regulates the antitumor reactivity of CD8 T cells, we bred *Maoa*-KO mice with *OT1* transgenic (*OT1*-Tg) mice and generated *OT1*-Tg/*Maoa*-KO mice producing OVA-specific CD8 T cells deficient in MAO-A (fig. S5A). We isolated OT1 T cells from either the *OT1*-Tg or *OT1*-Tg/*Maoa*-KO mice (denoted as OT1-WT or OT1-KO T cells, respectively) and separately transferred these cells into CD45.1 wild-type mice bearing preestablished B16-OVA tumors (Fig. 2D and fig. S5B). In this experiment, MAO-A deficiency comparison was confined solely to tumor-specific OT1 T cells. Both OT1-WT and OT1-KO T cells actively infiltrated tumors and showed an antigen-experienced phenotype ($CD44^{hi}CD62L^{lo}$; Fig. 2E and fig. S5, C and D). However, OT1-KO T cells were more effective in controlling tumor growth, corresponding with their enhanced effector function and reduced exhaustion phenotype (Fig. 2F and fig. S5, E to J). Collectively, these in vivo studies demonstrate that MAO-A works as an autonomous factor directly regulating CD8 T cell antitumor immunity.

MAO-A restrains the CD8 T cell response to antigen stimulation

Analysis of *Maoa* mRNA expression in tumor-infiltrating CD8 T cells showed an induction of the *Maoa* gene in these T cells compared with naïve CD8 T cells (Fig. 3A). Further analysis of tumor-infiltrating CD8 T cell subsets revealed that *Maoa* gene expression levels were positively correlated with the exhaustion and dysfunction status of these T cells: Compared with $PD\text{-}1^{lo}$ cells, $PD\text{-}1^{hi}$ "exhausted" T cells expressed higher levels of *Maoa* mRNA, and the $PD\text{-}1^{hi}$ cells coexpressing T cell immunoglobulin mucin 3 (Tim-3) and lymphocyte activation gene 3 protein (LAG-3), which were considered "most exhausted", expressed the highest levels of *Maoa* mRNA (Fig. 3A) (*18*, *19*). These in vivo data suggest that *Maoa* may be induced by tumor antigen recognition and then act as a negative-feedback regulator inhibiting CD8 T cell antitumor reactivity.

To test this hypothesis, we isolated CD8 T cells from *Maoa*-WT or *Maoa*-KO mice and then stimulated these T cells in vitro with anti-CD3, mimicking tumor antigen stimulation. We observed an induction of *Maoa* mRNA expression in *Maoa*-WT CD8 T cells, in agreement with previous reports; minimal *Maoa* mRNA expression was detected in *Maoa*-KO CD8 T cells, confirming their *Maoa* deficiency phenotype (Fig. 3B) (*20*). The induction of MAO-A protein expression in *Maoa*-WT CD8 T cells was also confirmed by Western blot analysis; the MAO-A isoenzyme, MAO-B, was not detected in CD8 T cells (fig. S6A). Compared with their *Maoa*-WT counterparts, *Maoa*-KO CD8 T cells showed an enhancement in almost all aspects of T cell activation, including cell proliferation (Fig. 3C), surface activation marker up-regulation (i.e., CD25; Fig. 3, D and E), effector cytokine production [i.e., interleukin-2 (IL-2) and IFN-γ; Fig. 3, F and G], and cytotoxic molecule production (i.e., Granzyme B; Fig. 3, H and I). Study of *Maoa*-KO OVA-specific OT1 T cells gave similar results, suggesting a general role of MAO-A in regulating CD8 T cells of diverse antigen specificities (fig. S7, A to D); study of *Maoa*-KO CD8 T cells stimulated with both anti-CD3 and anti-CD28 also yielded similar results, suggesting a general role of MAO-A in regulating CD8 T cell responses in the presence or absence of costimulation (fig. S6, B to I). To verify whether MAO-A deficiency directly contributed to the hyperresponsiveness of the *Maoa*-KO CD8 T cells, we performed a rescue experiment. We constructed a MIG [murine stem cell virus–internal ribosomal entry site–green fluorescent protein (MSCV-IRES-GFP)]-*Maoa* retroviral vector, used this vector to transduce *Maoa*-KO CD8 T cells, and achieved overexpression of MAO-A in these T cells (Fig. 3, J to L). MAO-A overexpression significantly reduced the hyperactivation of *Maoa*-KO CD8 T cells and their expression of multiple effector genes (i.e., *Il2*, *Ifng*, and *Gzmb*; Fig. 3, M to O). Together, these results indicate that MAO-A acts as a negative-feedback regulator restraining the CD8 T cell response to antigen stimulation.

MAO-A regulates CD8 T cell autocrine serotonin signaling

Next, we sought to investigate the molecular mechanisms mediating MAO-A restraint of CD8 T cell response to antigen stimulation. MAO-A is well known for its function in the brain where it breaks down neuron-produced serotonin, thereby regulating neuronal activity

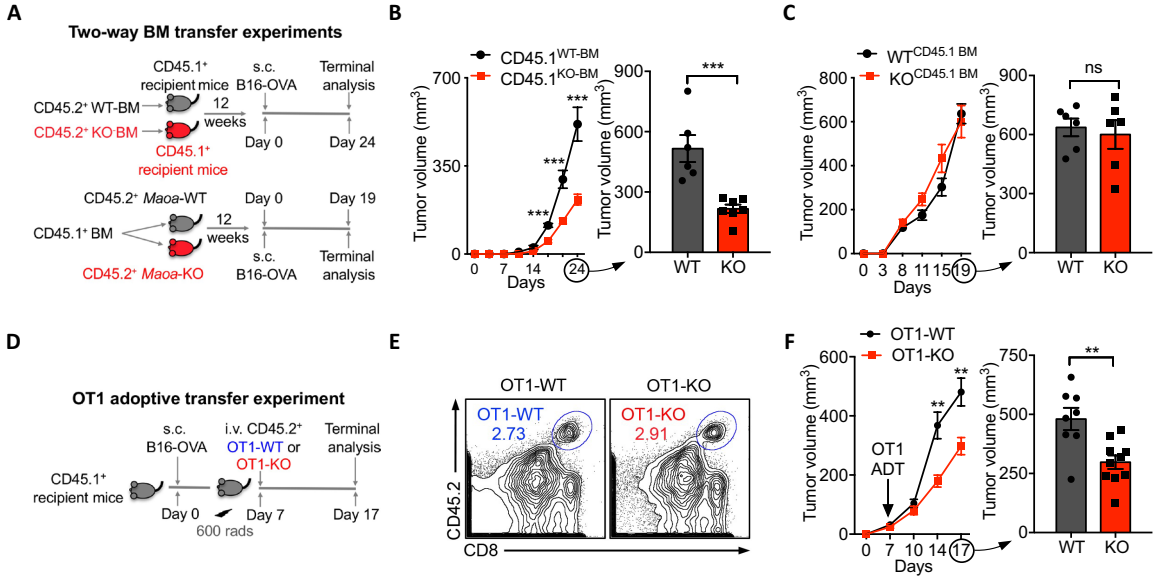

Fig. 2. MAO-A directly regulates CD8 T cell antitumor immunity. (**A** to **C**) Two-way BM transfer experiments. (A) Experimental design. (B) B16-OVA tumor growth in CD45.1 wild-type recipient mice reconstituted with BM cells from CD45.2 *Maoa*-WT or *Maoa*-KO donor mice (denoted as $CD45.1^{WT\text{-}BM}$ or $CD45.1^{KO\text{-}BM}$ mice, respectively) ($n = 6$ and 7). (C) B16-OVA tumor growth in CD45.2 *Maoa*-WT or *Maoa*-KO recipient mice reconstituted with BM cells from CD45.1 wild-type donor mice (denoted as $WT^{CD45.1\ BM}$ or $KO^{CD45.1\ BM}$ mice, respectively) ($n = 6$). (**D** to **F**) OT1 T cell adoptive transfer experiment ($n = 8$ to 10). i.v., intravenous. (D) Experimental design. OT1, OVA-specific transgenic CD8 T cell; OT1-WT, wild-type OT1 T cell; OT1-KO, MAO-A–deficient OT1 T cell. (E) FACS plots showing the detection of intratumoral OT1-WT and OT1-KO T cells (gated as $CD45.2^+CD8^+$ cells) in day 17 B16-OVA tumors. (F) Tumor growth. Representative of two experiments. ADT, adoptive transfer. Data are presented as the means ± SEM. $^{**}P < 0.01$ and $^{***}P < 0.001$ by Student's *t* test.

(*8*, *9*). CD8 T cells have been reported to synthesis serotonin, and serotonin has been implicated as an accessory signal to enhance T cell activation by signaling through T cell surface serotonin receptors [5-hydroxytryptamine receptors (5-HTRs)] (*20*–*22*). We therefore postulated that MAO-A might regulate CD8 T cell activity through modulating T cell autocrine serotonin production and signaling (Fig. 4A).

To test this hypothesis, we cultured *Maoa*-WT and *Maoa*-KO CD8 T cells in vitro, stimulated them with anti-CD3 to mimic antigen stimulation, and then analyzed their autocrine serotonin signaling pathway. After antigen stimulation, *Maoa*-WT CD8 T cells up-regulated the expression of the *Tph1* gene, which encodes the rate-limiting enzyme controlling serotonin synthesis, and also the expression of the *Maoa* gene, which would induce serotonin degradation, indicating the presence of an antigen stimulation–induced serotonin synthesis/degradation loop in CD8 T cells (Fig. 4, A to C). Considering the function of MAO-A, we speculated that MAO-A deficiency would not interfere with the serotonin synthesis arm but would impede the serotonin degradation arm, leading to enhanced secretion of serotonin by CD8 T cells. Compared with their wild-type counterparts, *Maoa*-KO CD8 T cells expressed comparable levels of *Tph1* but secreted much higher levels of serotonin after antigen stimulation (Fig. 4, B and D). Pharmacological inhibition of MAO-A in *Maoa*-WT CD8 T cells using an established MAOI, phenelzine, recapitulated the serotonin overproduction phenotype of *Maoa*-KO CD8 T cells (Fig. 4E). Correspondingly, phenelzine treatment of *Maoa*-WT CD8 T cells recapitulated the hyperactivation phenotype of *Maoa*-KO CD8 T cells, shown by increased production of the effector cytokines IL-2 and IFN-γ (Fig. 4, F and G). Supplementing serotonin to *Maoa*-WT CD8 T cells resulted in T cell hyperactivation and elevated production of IL-2 and IFN-γ (Fig. 4, H and I), whereas blocking T cell surface 5-HTRs using the antagonist asenapine eliminated the cytokine production difference between *Maoa*-WT and *Maoa*-KO CD8 T cells (Fig. 4, J and K). Serotonin has been reported to enhance T cell activation by signaling through the mitogen-activated protein kinase (MAPK) pathway that cross-talks with the T cell receptor (TCR) signaling pathways (*21*). We compared the signaling pathways in *Maoa*-WT and *Maoa*-KO CD8 T cells after antigen stimulation and found that *Maoa*-KO T cells showed an enhancement of MAPK signaling [i.e., extracellular signal–regulated kinase (ERK) phosphorylation; Fig. 4L and fig. S8, B and C] and TCR downstream signaling [i.e., nuclear translocation of nuclear factor of activated T cells (NFAT), nuclear factor κB (NF-κB), and c-Jun transcription factors; Fig. 4M and fig. S8, D to I]; this enhancement was largely abrogated by blocking 5-HTRs (Fig. 4, L and M, and fig. S8, B to I). There are multiple 5-HTR family members; in mice, there are 13 5-HTR family members (*21*). Analyses of the expression of all 13 5-HTR genes in CD8 T cells before and after anti-CD3 stimulation revealed that these cells predominantly expressed 2 of the 13 5-HTR genes: *Htr2b* and *Htr7*; there was a further up-regulation of *Htr7* after anti-CD3 stimulation (fig. S8J). These data suggest that serotonin signaling in mouse CD8 T cells may mainly be mediated through Htr2b and Htr7; in particular, Htr7 may mediate the activation-related signaling events. Collectively, these in vitro data suggest that MAO-A regulates CD8 T cell activation through modulating T cell autocrine serotonin production and signaling (Fig. 4A and fig. S8A).

To validate this working model in vivo, we directly measured intratumoral serotonin in *Maoa*-KO and *Maoa*-WT mice, as well as in wild-type mice treated or untreated with phenelzine. Consistent with the in vitro results, increased levels of serotonin were detected specifically in tumors collected from the *Maoa*-KO mice (Fig. 4N)

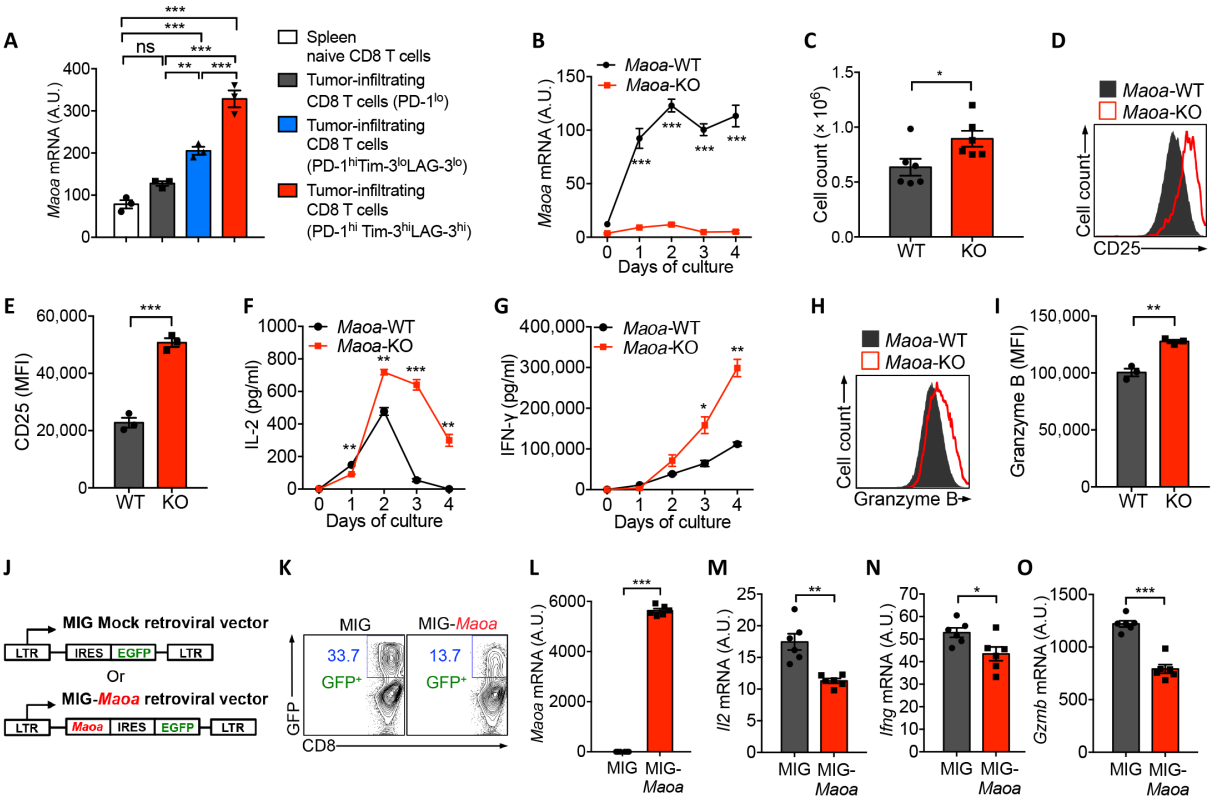

Fig. 3. MAO-A acts as a negative-feedback regulator to restrain CD8 T cell activation. (**A**) qPCR analyses of *Maoa* mRNA expression in tumor-infiltrating CD8 T cell subsets isolated from day 14 B16-OVA tumors grown in wild-type B6 mice ($n = 3$). Naïve CD8 T cells (gated as TCRβ$^+$CD8$^+$CD44^{lo}CD62L^{hi} cells) sorted from the spleen of tumor-free B6 mice were included as controls. (**B** to **I**) Activation of *Maoa*-WT and *Maoa*-KO CD8 T cells ($n = 3$ to 6). CD8 T cells were purified from *Maoa*-WT and *Maoa*-KO mice and stimulated in vitro with anti-CD3. The analyses of *Maoa* mRNA expression (B), cell proliferation (C), activation marker expression [i.e., CD25 (D and E)], effector cytokine production [i.e., IL-2 (F) and IFN-γ (G)], and cytotoxic molecule production [i.e., Granzyme B (H and I)] are shown, either over a 4-day time course (B, F, and G) or at day 3 after anti-CD3 stimulation (C to E, H, and I). (**J** to **O**) Activation of *Maoa*-KO CD8 T cells with MAO-A overexpression ($n = 6$). LTR, long terminal repeats; EGFP, enhanced green fluorescent protein. CD8 T cells were isolated from *Maoa*-KO mice, stimulated in vitro with anti-CD3 and transduced with a MIG-*Maoa* retrovector or a MIG mock retrovector (J). The analyses of retroviral transduction efficiency (K), *Maoa* mRNA expression (L), effector cytokine mRNA expression [i.e., *Il2* (M) and *Ifng* (N)], and cytotoxicity molecule mRNA expression [i.e., *Gzmb* (O)] at day 4 after stimulation are presented. Representative of two (A and J to O) and three (B to I) experiments. Data are presented as the means ± SEM. *$P < 0.05$, **$P < 0.01$, and ***$P < 0.001$ by one-way ANOVA (A) or by Student's *t* test (B, C, E to G, I, and L to O).

and phenelzine-treated *Maoa*-WT mice (Fig. 4O). Depletion of CD8 T cells in *Maoa*-WT mice largely abolished the phenelzine treatment–induced accumulation of serotonin in the tumor, indicating that tumor-infiltrating CD8 T cells are major producers of serotonin in the tumor and that this is negatively regulated by MAO-A (Fig. 4O and fig. S8L). There were no significant changes in serotonin levels in serum under any conditions (fig. S8, K and M), suggesting that MAO-A regulation of serotonin in the tumor is largely a local effect, resembling MAO-A regulation of serotonin in the brain (*8*, *9*).

Together, these in vitro and in vivo data support a working model that MAO-A negatively regulates CD8 T cell antitumor immunity, at least partly, through modulating CD8 T cell autocrine serotonin signaling in the tumor.

MAO-A blockade for cancer immunotherapy

The identification of MAO-A as a new immune checkpoint negatively regulating CD8 T cell antitumor immunity marks it as a promising drug target for developing new forms of ICB therapy. Because of MAO-A's well-characterized function in the brain, small-molecule MAOIs have been developed and clinically used for treating depression symptoms, making it a highly feasible and attractive approach to repurpose these established MAOI antidepressants for cancer immunotherapy (*23*). Some MAOIs cross-inhibit the MAO-A isoenzyme MAO-B; however, only MAO-A effectively degrades serotonin, and all MAOIs exhibit their antidepressant function mainly through inhibiting MAO-A enzyme activity, thereby regulating serotonin signaling in the brain (*14*, *23*). When tested in vitro, multiple MAOIs efficiently induced CD8 T cell hyperactivation (i.e., up-regulated expression of CD25, Granzyme B, IL-2, and IFN-γ; Fig. 5A and fig. S9, A to F). When tested in vivo in a B16-OVA melanoma prevention model, these MAOIs markedly suppressed tumor growth (Fig. 5, B and C). The MAOIs that we tested were phenelzine, clorgyline, and moclobemide, covering the major categories of established MAOIs classified on the basis of whether they are nonselective or selective for MAO-A and whether their effect is reversible (fig. S9A) (*23*). Among these MAOIs, phenelzine (trade name: Nardil) is clinically available in the United States (*23*). In the following studies, we chose phenelzine as a representative to further evaluate the cancer therapy potential of MAOI drugs.

First, we studied the efficacy of phenelzine in treating preestablished B16-OVA melanoma solid tumors and found that phenelzine treatment effectively suppressed tumor progression (Fig. 5, D and E).

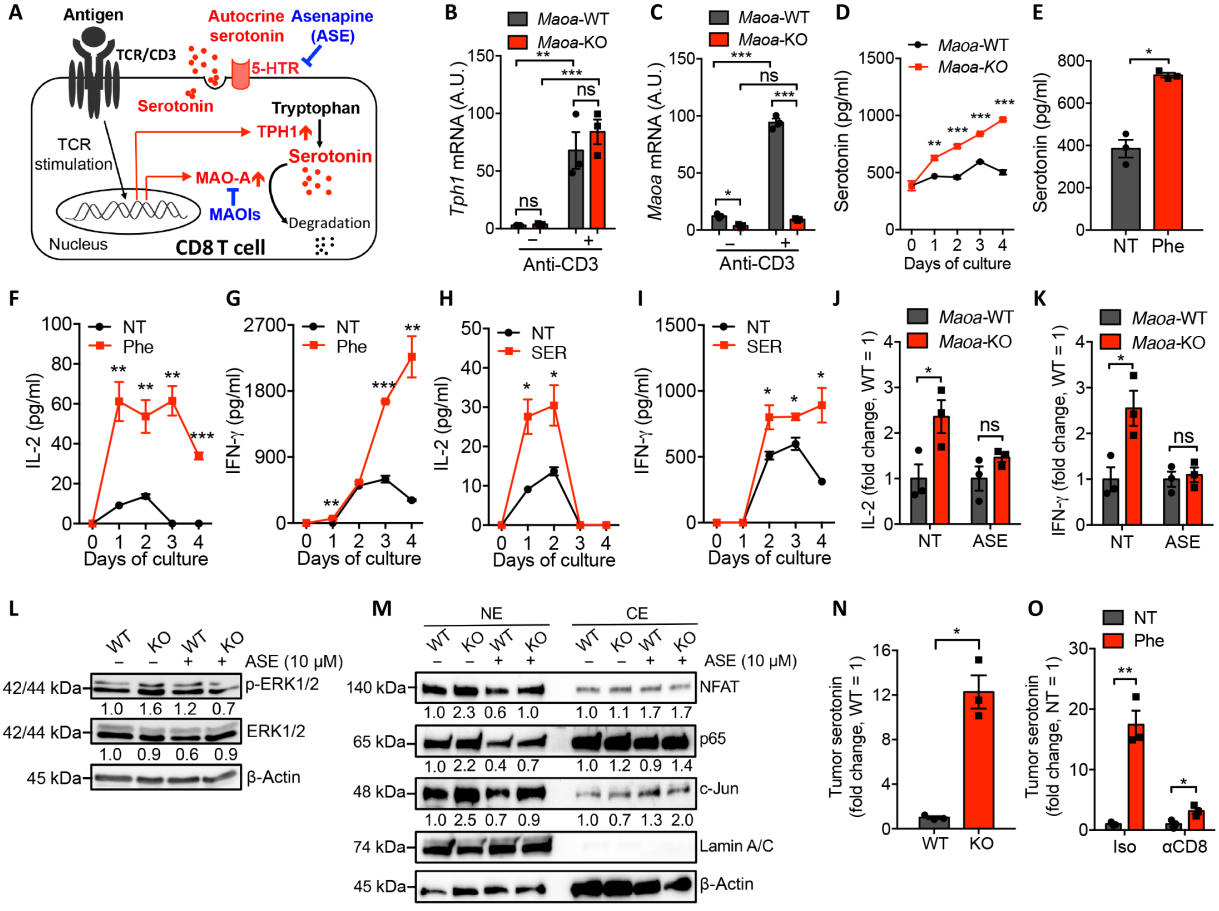

Fig. 4. MAO-A regulates CD8 T cell autocrine serotonin signaling. (**A**) Schematics showing the antigen stimulation-induced serotonin synthesis/degradation loop in a CD8 T cell. Possible pharmacological interventions are indicated. ASE, asenapine (an antagonist blocking a majority of 5-HTRs). (**B** and **C**) qPCR analyses of *Tph1* (B) and *Maoa* (C) mRNA expression in *Maoa*-WT and *Maoa*-KO CD8 T cells, at 24 hours after anti-CD3 stimulation ($n = 3$). (**D** and **E**) CD8 T cell serotonin production in vitro ($n = 3$). (D) Serotonin levels in *Maoa*-WT and *Maoa*-KO CD8 T cell cultures over a 4-day time course after anti-CD3 stimulation. (E) Serotonin levels in *Maoa*-WT CD8 T cell cultures at 24 hours after anti-CD3 stimulation, with or without phenelzine treatment [Phe or no treatment (NT)]. Serotonin levels were measured by ELISA. (**F** to **K**) CD8 T cell effector cytokine production in vitro ($n = 3$). (F and G) IL-2 and IFN-γ levels in *Maoa*-WT CD8 T cell cultures over a 4-day time course after anti-CD3 stimulation, with or without phenelzine (Phe) treatment (Phe or NT). (H and I) IL-2 and IFN-γ levels in *Maoa*-WT CD8 T cell cultures over a 4-day time course after anti-CD3 stimulation, with or without serotonin (SER) treatment (SER or NT). (J and K) IL-2 and IFN-γ levels in *Maoa*-WT and *Maoa*-KO CD8 T cell cultures at day 2 after anti-CD3 stimulation, with or without asenapine treatment (ASE or NT). Cytokine levels were measured by ELISA. (**L** and **M**) CD8 T cell 5-HTR and TCR signaling cross-talk in vitro. *Maoa*-WT and *Maoa*-KO CD8 T cells were stimulated with anti-CD3 for 2 days in the presence or absence of asenapine. Cells were then rested on ice for 2 hours and restimulated with anti-CD3 for 20 min, followed by total protein extraction (L) or nuclear protein extraction and cytoplasmic protein extraction (NE and CE; M) and Western blot analysis of key signaling molecules involved in 5-HTR (L) and TCR (M) signaling pathways. (**N** and **O**) CD8 T cell serotonin production in vivo in a B16-OVA melanoma model ($n = 3$). On day 14 after tumor challenge, tumors were collected from experimental mice for serotonin measurement using HPLC. (N) Intratumoral serotonin levels in *Maoa*-WT and *Maoa*-KO mice (denoted as WT and KO, respectively). (O) Intratumoral serotonin levels in *Maoa*-WT mice, with or without phenelzine treatment (Phe or NT) and with or without antibody-induced depletion of CD8 T cells (αCD8 or Iso). Representative of two (L to O) and three (B to K) experiments. Data are presented as the means ± SEM. $^*P < 0.05$, $^{**}P < 0.01$, and $^{***}P < 0.001$, by two-way ANOVA (B and C) or by Student's *t* test (D to K, N, and O).

This MAOI-induced tumor suppression effect was mediated by CD8 T cells, because no tumor suppression was observed when we depleted CD8 T cells in tumor-bearing B6 wild-type mice (fig. S10, A and B). Correspondingly, analysis of total tumor-infiltrating CD8 T cells under phenelzine treatment showed a hyperactivation phenotype of these T cells, evidenced by their enhanced production of effector molecules (i.e., IFN-γ and Granzyme B; Fig. 5, F to I) and reduced expression of exhaustion markers (i.e., PD-1; Fig. 5, J and K); analysis of tumor antigen-specific CD8 T cells (i.e., OVA^+ T cells) showed the similar results (fig. S10, I to P). To further study the impact of phenelzine treatment on antitumor T cell exhaustion, we tracked the PD-1–positive subpopulation of tumor-infiltrating CD8 T cells over time; we detected a significant decrease of the PD-1–positive subpopulation in phenelzine-treated mice (fig. S10, C and D). Functional analysis showed an enhanced production of effector molecules (i.e., IFN-γ and Granzyme B) in PD-1–positive subpopulations under phenelzine treatment (fig. S10, E to H). Therefore, MAO-A blockade could alleviate T cell exhaustion and improve the overall effector function of tumor-infiltrating CD8 T cells.

Next, we studied the potential of phenelzine treatment for combination therapy, particularly combining with other ICB therapies such as the PD-1/PD-L1 blockade therapy (Fig. 5L) (*6*). In the MC38 colon cancer model, which is sensitive to immunotherapy, phenelzine treatment completely suppressed tumor growth as effectively as the

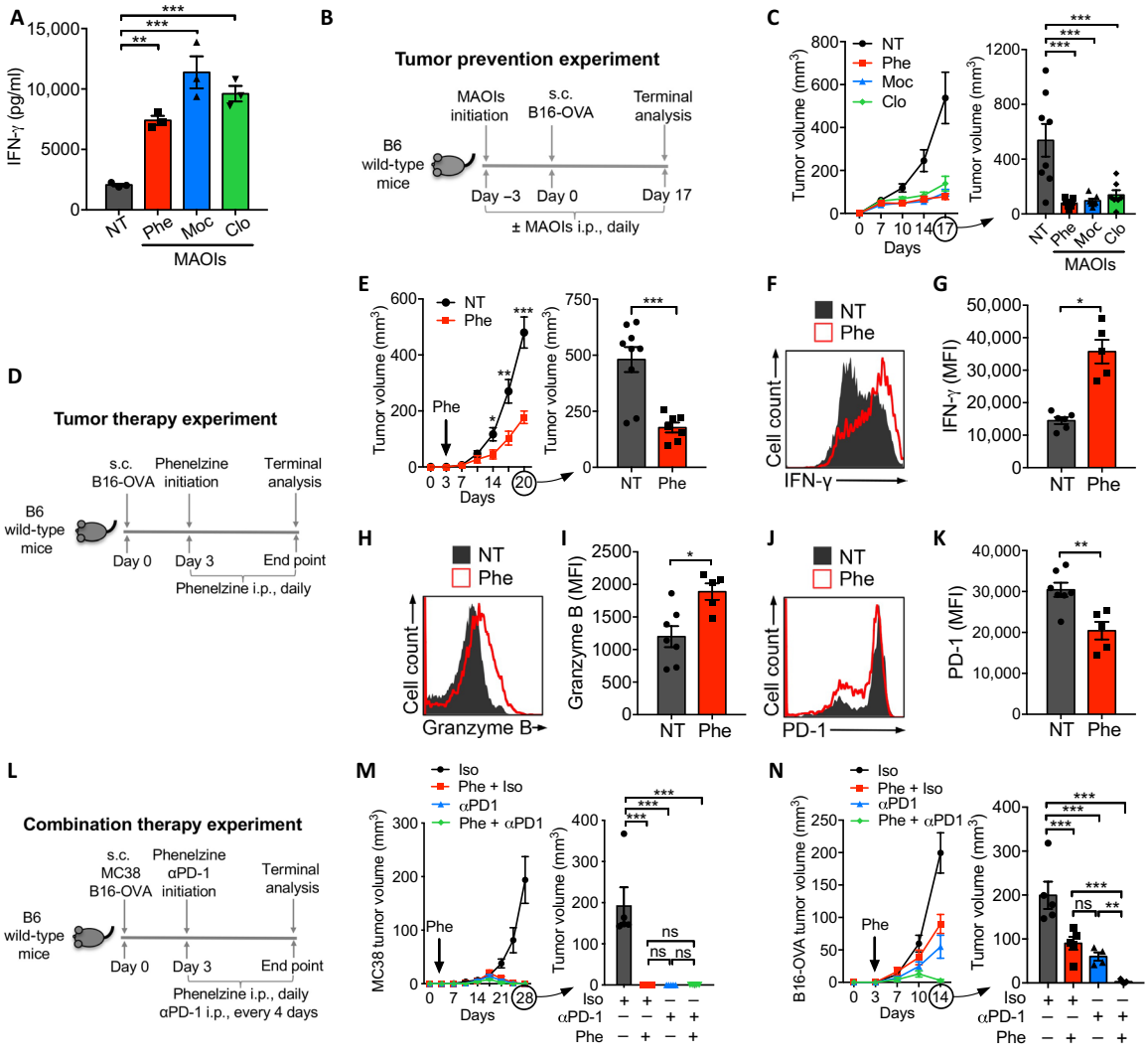

Fig. 5. MAO-A blockade for cancer immunotherapy: Syngeneic mouse tumor model studies. (**A**) Effect of MAOI treatment on CD8 T cell activation in vitro. CD8 T cells were purified from B6 wild-type mice and stimulated with anti-CD3 for 3 days in the absence (NT) or presence of MAOIs (Phe; Moc, moclobemide; Clo, clorgyline). ELISA analyses of IFN-γ production are presented ($n = 3$). (**B** and **C**) Cancer therapy potential of MAOI treatment in a B16-OVA melanoma model. i.p., intraperitoneal. (B) Experimental design. B6 wild-type mice were untreated (NT) or treated with MAOIs (Phe, Moc, and Clo). (C) Tumor growth ($n = 6$ to 8). (**D** to **K**) Cancer therapy potential of phenelzine treatment in a B16-OVA melanoma model. (D) Experimental design. (E) Tumor growth in B6 wild-type mice with or without phenelzine treatment (Phe or NT; $n = 7$ to 9). (F to K) Analysis of tumor-infiltrating CD8 T cells in B6 wild-type mice with or without phenelzine treatment. On day 20 after tumor inoculation, tumors were collected, followed by TII isolation and FACS analysis. The analyses of tumor-infiltrating CD8 T cells (pregated as $CD45.2^+TCR\beta^+CD8^+$ cells) for their intracellular production of effector cytokines [i.e., IFN-γ (F and G)] and cytotoxic molecules [i.e., Granzyme B (H and I)], and their surface expression of exhaustion markers [i.e., PD-1 (J and K)] are presented. (**L** to **N**) Cancer therapy potential of MAOI treatment in combination with anti–PD-1 treatment in a MC38 colon cancer model and a B16-OVA melanoma model. (L) Experimental design. B6 wild-type mice were inoculated with tumor cells, with or without phenelzine treatment and with or without anti–PD-1 treatment (Iso, Phe + Iso, αPD-1, or Phe + αPD-1). (M) MC38 tumor growth ($n = 5$). (N) B16-OVA tumor growth ($n = 4$ and 5). Representative of two (B, C, and L to N) and three (A, and D to K) experiments. Data are presented as the means ± SEM. $^*P < 0.05$, $^{**}P < 0.01$, and $^{***}P < 0.001$ by one-way ANOVA (A, C, M, and N) or by Student's *t* test (E to K).

anti–PD-1 treatment (Fig. 5M). In the B16-OVA melanoma model, which is less sensitive to immunotherapy, phenelzine treatment significantly suppressed tumor growth at a level comparable with the anti–PD-1 treatment; the combination of phenelzine and anti–PD-1 treatments yielded superior efficacy and totally suppressed tumor growth (Fig. 5N). These tumor suppression effects of phenelzine were likely mediated by its immune regulatory function, because phenelzine treatment did not affect the tumor cells themselves and did not suppress the growth of MC38 and B16-OVA tumors in immunodeficient NOD scid gamma (NSG) mice (fig. S11, A to D). Collectively, these syngeneic mouse tumor model studies provided proof-of-principle evidence for the cancer immunotherapy potential of MAOIs.

To explore the translational potential of MAO-A blockade therapy, we studied human CD8 T cells and confirmed that they also up-regulated *MAOA* gene expression after antigen stimulation, resembling their mouse counterparts (Fig. 6A). To directly evaluate whether MAOI treatment could enhance human CD8 T cell antitumor efficacy in vivo, we used a human T cell adoptive transfer and human tumor xenograft NSG mouse model (*24*). NY-ESO-1, a well-recognized tumor antigen common in many human cancers,

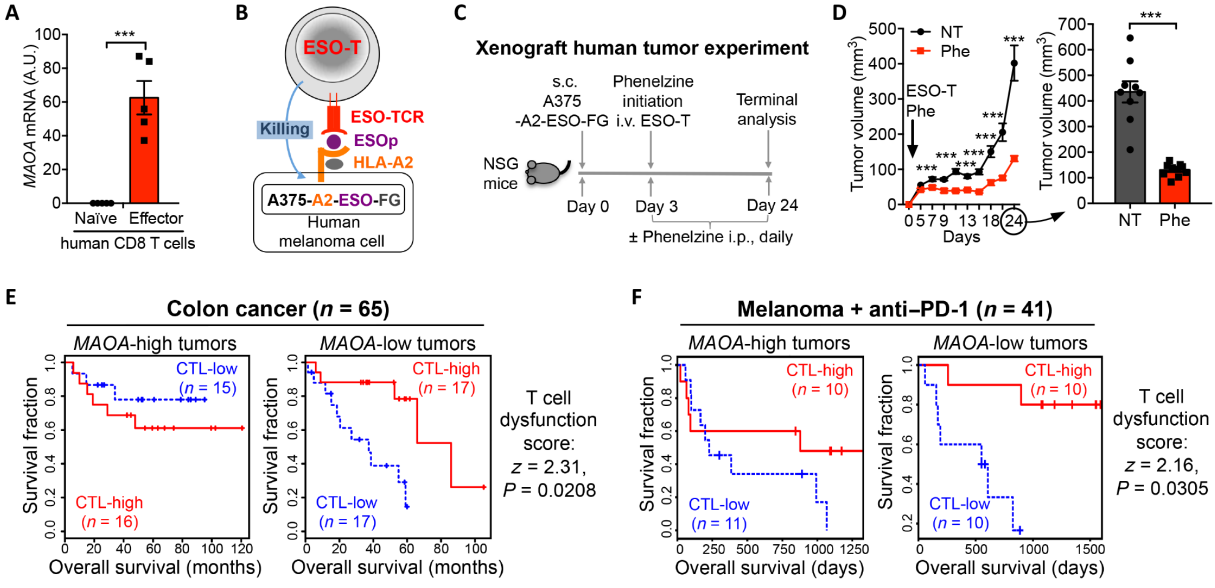

Fig. 6. MAO-A blockade for cancer immunotherapy: Human T cell and clinical data correlation studies. (**A** to **D**) Translational potential of MAOI treatment for improving human CD8 T cell antitumor reactivity. (A) qPCR analyses of *MAOA* mRNA expression in naïve and anti-CD3/anti-CD28 stimulated human CD8 T cells of random healthy donors ($n = 5$). (B) Schematics showing a human tumor–T cell pair designated for the study of human CD8 T cell antitumor reactivity. A375-A2-ESO-FG, a human A375 melanoma cell line engineered to express an NY-ESO-1 tumor antigen, its matching MHC molecule (HLA-A2), and a dual reporter comprising a firefly luciferase and an enhanced green fluorescence protein (FG). ESO-T, human peripheral blood CD8 T cells engineered to express an NY-ESO-1 antigen-specific TCR (ESO-TCR; clone 3A1). ESOp, NY-ESO-1 peptide. (C) Experimental design to study the cancer therapy potential of MAOI treatment in a human T cell adoptive transfer and human melanoma xenograft NSG mouse model. (D) Tumor growth from (C) ($n = 9$ and 10). (**E** and **F**) Clinical data correlation studies. A TIDE computational method was used to study the association between the tumor-infiltrating CD8 T cell (also known as cytotoxic T lymphocyte, CTL) level and overall patient survival in relation to the intratumoral *MAOA* gene expression level. For each patient cohort, tumor samples were divided into *MAOA*-high (samples with *MAOA* expression one standard derivation above the average; shown in left survival plot) and *MAOA*-low (remaining samples; shown in right survival plot) groups, followed by analyzing the association between the CTL levels and survival outcomes in each group. The CTL level was estimated as the average expression level of *CD8A*, *CD8B*, *GZMA*, *GZMB*, and *PRF1*. Each survival plot presented tumors in two subgroups: CTL-high group (red) had above-average CTL values among all samples, whereas CTL-low group (blue) had below-average CTL values. A T cell dysfunction score (z score) was calculated for each patient cohort, correlating the *MAOA* expression level with the beneficial effect of CTL infiltration on patient survival. A positive z score indicates that the expression of *MAOA* is negatively correlated with the beneficial effect of tumor-infiltrating CTL on patient survival. The P value indicates the comparison between the *MAOA*-low and *MAOA*-high groups and was calculated by two-sided Wald test in a Cox-PH regression. (E) TIDE analysis of a colon cancer patient cohort (GSE29621; $n = 65$). $z = 2.31$; $P = 0.0208$. (F) TIDE analysis of a melanoma patient cohort receiving anti–PD-1 treatment (ENA PRJEB23709; $n = 41$). $z = 2.16$, $P = 0.0305$. Representative of two experiments. Data are presented as the means ± SEM. ***$P < 0.001$ by Student's t test (A and D).

was chosen as the model tumor antigen (*24*). An A375 human melanoma cell line was engineered to coexpress NY-ESO-1 and its matching major histocompatibility complex (MHC) molecule, human leukocyte antigen serotype A2 (HLA-A2), to serve as the human tumor target; the cell line was also engineered to express a dual reporter comprising a firefly luciferase and an enhanced green fluorescence protein (denoted as A375-A2-ESO-FG) (*25*). A Retro/ESO-TCR retroviral vector was constructed to encode an NY-ESO-1–specific TCR (clone 3A1; denoted as ESO-TCR) and was used to transduce healthy donor peripheral blood CD8 T cells; the resulting T cells (denoted as ESO-T cells) expressed ESO-TCRs and specifically targeted A375-A2-ESO-FG tumor cells, thereby modeling the tumor-specific human CD8 T cells (Fig. 6B and fig. S12, A to D). A375-A2-ESO-FG cells were subcutaneously injected into NSG mice to establish solid tumors, followed by intravenous injection of ESO-T cells with or without phenelzine treatment (Fig. 6C). MAOI treatment effectively suppressed tumor growth; this therapeutic effect was mediated by tumor-specific ESO-T cells because no tumor suppression was observed in NSG mice that did not receive adoptive transfer of ESO-T cells (Fig. 6D and fig. S12, E and F). Collectively, this human xenograft tumor model study supports the translational potential of MAO-A blockade for cancer immunotherapy.

Last, we conducted clinical data correlation studies to investigate whether *MAOA* gene expression is correlated with CD8 T cell [also known as cytotoxic T lymphocyte (CTL)] antitumor activities and clinical outcomes in patients with cancer. A Tumor Immune Dysfunction and Exclusion (TIDE) computational method was used, which models the induction of CD8 T cell dysfunction in tumors by analyzing the interactions of three variants: (i) the intratumoral expression of a selected gene, (ii) the intratumoral level of CD8 T cells, and (iii) patient survival (*26*). *MAOA* expression level was negatively correlated with the beneficial effect of tumor-infiltrating CD8 T cell on patient survival in multiple cancer patient cohorts spanning colon cancer (Fig. 6E) (*27*), lung cancer (fig. S13A) (*28*), cervical cancer (fig. S13B) (*29*), and pancreatic cancer (fig. S13C) (*30*). Moreover, analysis of a melanoma patient cohort receiving anti–PD-1 treatment showed that high levels of intratumoral *MAOA* expression largely abrogated the patient survival benefit offered by tumor-infiltrating CD8 T cells, suggesting that combining MAO-A blockade therapy with PD-1/PD-L1 blockade therapy may provide synergistic therapeutic benefits through further activating tumor-infiltrating CD8 T cells (Fig. 6F) (*31*). These whole-tumor lysate transcriptome data analyses could not localize the *MAOA* expression to a specific cell type (i.e., CD8 T cells); future studies of quality transcriptome data

generated from single cells or sorted tumor-infiltrating CD8 T cells are needed to produce such information. Nonetheless, the present clinical data correlation studies identified MAO-A as a possible negative regulator of CD8 T cell antitumor function in a broad range of patients with cancer, including those receiving existing ICB therapies, suggesting MAO-A as a potential drug target for developing new forms of ICB therapy and combination therapy. Together, these preclinical animal studies and clinical data correlation studies suggest that MAO-A is a promising new drug target of T cell–based cancer immunotherapy and that repurposing of established MAOI antidepressants is a promising path to develop MAO-A blockade immunotherapy.

DISCUSSION

On the basis of our findings, we propose an "intratumoral MAO-A–serotonin axis" model to elucidate the role of MAO-A in regulating CD8 T cell antitumor immunity (fig. S14). Analogous to the well-characterized MAO-A–serotonin axis in the brain, where MAO-A controls the availability of serotonin in a neuron-neuron synapse, thereby regulating neuronal activity, the "MAO-A–serotonin axis" in a tumor controls the availability of serotonin in a tumor cell–T cell immune synapse, thereby regulating antitumor T cell reactivity (fig. S14). The resemblance is notable, considering that both the nervous system and the immune system are evolved to defend a living organism by sensing and reacting to environmental danger, externally and internally, including tissue traumas, infections, and malignancies (*32*). Despite their distinct anatomic structures, the nervous system has a fixed organization, whereas the immune system comprises mobile and disperse cells; from an evolutionary point of view, it makes sense that some critical molecular regulatory pathways are preserved for both defense systems. Neurons and immune cells share a broad collection of signal transducers, surface receptors, and secretory molecules (*32*). In particular, many neurotransmitters and neuropeptides traditionally considered specific for neurons are expressed in immune cells, although their functions in the immune system are, to a large extent, still unknown (*33*). Studying this group of molecules and their regulatory circuits in tumor immunology thus may provide new opportunities for generating knowledge and identifying new drug targets for developing next-generation cancer immunotherapies; our current finding of this MAO-A–serotonin axis regulation of CD8 T cell antitumor immunity can be such an example.

Our study showed that *Maoa* expression was induced by antigen-TCR stimulation in CD8 T cells and, in turn, restrained T cell activation (Fig. 3). This negative-feedback loop qualifies MAO-A as an immune checkpoint and adds it to the expanding immune checkpoint family comprising PD-1/PD-L1, CTLA-4, Tim-3, LAG-3, T cell immunoreceptor with Ig and ITIM domains (TIGIT), V-domain Ig suppressor of T cell activation (VISTA), and others (*4*). However, MAO-A is unique in this group because it is already a well-established drug target due to its known function in the brain (*23*). Small-molecule MAOIs have been developed to block MAO-A activity, thereby regulating serotonin signaling in the brain, and were the first drugs approved for treating depression (*23*). In our study, we tested multiple clinically approved MAOIs (phenelzine, moclobemide, and clorgyline) and demonstrated their T cell–enhancing and tumor suppression effects in preclinical animal models, pointing to the possibility of repurposing these drugs for cancer immunotherapy (Fig. 5 and fig. S9). Developing new cancer drugs is extremely costly and time consuming; drug repurposing offers an economic and speedy pathway to additional cancer therapies, because approved drugs have known safety profiles and modes of actions and thus can enter the clinic quickly (*34*). MAOIs were introduced in the 1950s and were used extensively over the subsequent two decades, but since then, their use has dwindled because of reported side effects and the introduction of other classes of antidepressant agents (*23*). However, these MAOI side effects were vastly overstated and should be revisited (*23*). For instance, a claimed major side effect of MAOIs is their risk of triggering tyramine-induced hypertensive crisis when patients eat tyramine-rich foods such as aged cheese (hence, "the cheese effects"); this concern led to cumbersome food restrictions that are now considered largely unnecessary (*23*). A transdermal delivery system for selegiline (Emsam) has also been developed that can largely avoid potential food restrictions (*23*). Therefore, interest in MAOIs as a major class of antidepressants is reviving (*23*), and repurposing MAOIs for cancer immunotherapy can be an attractive new application of these potent drugs.

Depression and anxiety are common in patients with cancer: Prevalent rates of major depression among patients with cancer are four times higher than the general population, and up to a quarter of patients with cancer have clinically significant depression and anxiety symptoms (*35*). Repurposing MAOIs for cancer immunotherapy thus may provide patients with cancer with dual antidepressant and antitumor benefits. A large majority of antidepressants, including MAOIs, selective serotonin reuptake inhibitors (SSRIs), serotonin modulators and stimulators (SMSs), serotonin antagonists and reuptake inhibitors (SARIs), and serotonin-norepinephrine reuptake inhibitors (SNRIs), all work through regulating serotonin signaling in the brain via inhibiting the various key molecules that control serotonin degradation, reuptake, and detection (*36*). Our study revealed the existence of a MAO-A–serotonin axis in tumors that regulates CD8 T cell antitumor immunity (fig. S14). It is plausible to postulate that the other key serotonin regulatory molecules that function in the brain may also function in the tumor regulating T cell antitumor immunity (*36*). A recent nationwide cohort study in Israel reported that adherence to antidepressant medications is associated with reduced premature mortality in patients with cancer (*35*). Another clinical study reported lymphocyte subset changes associated with antidepressant treatments in patients with a major depression disorder (*37*). Studying patients with cancer for possible correlations between antidepressant treatments, antitumor immune responses, and clinical outcomes therefore might yield valuable knowledge informing the immune regulatory function of antidepressants and instructing the potential repurposing of select antidepressant drugs for cancer immunotherapy.

In our study, we found that *Maoa* gene was highly expressed in tumor-infiltrating CD8 T cells, with the most "exhausted" cells (PD-1^{hi}Tim-3^{hi}LAG-3^{hi}) expressing the highest levels of *Maoa*, suggesting that these cells may benefit the most from the MAOI treatment (*18*, *19*). We also found that MAO-A regulated CD8 T cell antitumor immunity, at least partly, through modulating the serotonin-MAPK pathway, which is nonredundant to other major immune checkpoint regulatory pathways, suggesting that MAOI treatment can be a valuable component for combination therapy (*4*). MAOI treatment synergized with anti–PD-1 treatment in suppressing syngeneic mouse tumor growth, and *MAOA* expression levels dictated patient survival in patients with melanoma receiving anti–PD-1 therapy (Figs. 5 and 6). Patients undergoing cancer treatment,

including traditional chemo/radio therapies and the new immunotherapies such as ICB therapies, often report incurred or exacerbated depression symptoms; these central nervous system (CNS) side effects are considered to be associated with treatment-induced immune reaction and inflammation (*38*–*40*). Adding MAOIs with antidepressant function to a combination cancer therapy thus may both improve antitumor efficacy and alleviate CNS side effects. Some earlier studies reported that MAOIs can directly suppress the growth of androgen-sensitive and castration-resistant prostate cancer cells, presumably through regulating cancer cell autophagy and apoptosis, suggesting additional mechanisms that MAOIs may deploy to target certain cancers (*41*, *42*).

In summary, here, we identified MAO-A as an immune checkpoint and demonstrated the potential of repurposing established MAOI antidepressants for cancer immunotherapy. The notion that *MAOA*, "the warrior gene," not only acts in the brain to regulate the aggressiveness of human behavior but also acts in a tumor to control the aggressiveness of antitumor immunity is interesting. Future clinical studies are encouraged to investigate the clinical correlations between MAOI treatment and clinical outcomes in patients with cancer and to explore the possibility of repurposing MAOIs for combination cancer immunotherapy. Meanwhile, the immune regulatory function of MAO-A certainly goes beyond regulating CD8 T cells. We have detected MAO-A expression in other immune cells (e.g., dendritic cells, macrophages, and regulatory T cells); and in *Maoa*-KO mice, we have observed the hyperresponsiveness of multiple immune cells in various mouse tumor models. It is also likely that MAO-A regulates immune reactions to multiple diseases beyond cancer, such as infections and autoimmune diseases. Studying the roles of MAO-A in regulating various immune cells under different health and disease conditions will be interesting topics for future research.

MATERIALS AND METHODS

Study design

To search for new drug targets regulating antitumor immunity, we isolated TIIs from B16-OVA melanoma tumors and evaluated TII gene expression profiles; we detected a significant change in *Maoa* gene expression. To study MAO-A as an autologous factor regulating antitumor CD8 T cell immunity, we conducted a series of in vivo tumor experiments involving multiple syngeneic mouse tumor models (i.e., B16-OVA melanoma and MC38 colon cancer models), *Maoa*-KO mice, as well as BM and T cell adoptive transfer approaches. Tumor growth was monitored, and the tumor-infiltrating CD8 T cells were analyzed using flow cytometry and scRNA-seq. To investigate the MAO-A regulation of CD8 T cell activation through modulating T cell autocrine serotonin, we stimulated *Maoa*-KO and *Maoa*-WT CD8 T cells in vitro and compared their T cell activation, TCR signaling, and serotonin secretion and signaling using flow cytometry, enzyme-linked immunosorbent assay (ELISA), qPCR, and Western blot; serotonin modulation was also validated in vivo in the B16-OVA melanoma model using high-performance liquid chromatography (HPLC). To evaluate the potential of repurposing MAOI antidepressants for cancer immunotherapy, we studied the T cell regulatory and antitumor effects of MAOI treatment in vitro in T cell culture and in vivo in B16-OVA and MC38 tumor models alone or in combination with anti–PD-1 treatment. To explore the translational potential of MAO-A blockade therapy, we examined the *MAOA* gene expression in primary human CD8 T cells and studied the therapeutic effects of MAOI treatment in a human T cell adoptive transfer and human melanoma xenograft NSG mouse model. Last, we conducted clinical data correlation studies and investigated the correlation of intratumoral *MAOA* gene expression with CD8 T cell antitumor activities and clinical outcomes in multiple cancer patient cohorts spanning melanoma, colon cancer, lung cancer, cervical cancer, and pancreatic cancer.

Mice

C57BL/6J (B6), B6.SJL-*Ptprc*^{a}*Pepc*^{b}/BoyJ (CD45.1), 129S-*Maoa*^{tm1Shih}/J (*Maoa*-KO) (*15*), C57BL/6-Tg (TcraTcrb)1100Mjb/J (*OT1*-Tg), and NOD.Cg-*Prkdc*^{scid} *Il2rg*^{tm1Wjl}/SzJ (Nod scid gamma or NSG) mice were purchased from the Jackson Laboratory (JAX; Bar Harbor). The *OT1*-Tg mice deficient of *Maoa* (*OT1*-Tg/*Maoa*-KO) were generated at the University of California, Los Angeles (UCLA) through breeding *OT1*-Tg mice with *Maoa*-KO mice. All animals were maintained in the animal facilities at UCLA. Eight- to 12-week-old females were used for all experiments unless otherwise indicated. All animal experiments were approved by the Institutional Animal Care and Use Committee of UCLA.

Cell lines

The B16-OVA mouse melanoma cell line and the PG13 retroviral packaging cell line were provided by P. Wang (University of Southern California, CA, USA) (*43*). The MC38 mouse colon adenocarcinoma cell line was provided by M. Bosenberg (Yale University, CT, USA) (*44*). The human embryonic kidney 293T and Phoenix-ECO retroviral packaging cell lines were purchased from the American Type Culture Collection (ATCC). The A375-A2-ESO-FG human melanoma cell line was previously reported (*24*, *25*). The Phoenix-ECO-MIG, Phoenix-ECO-MIG-*Maoa*, and PG13-ESO-TCR stable virus producing cell lines were generated in this study.

Viral vectors

The MIG retroviral vector was reported previously (*45*). MIG-*Maoa* and Retro/ESO-TCR retroviral vectors were generated in this study.

Media and reagents

Adherent cell culture medium (denoted as D10 medium) was made of Dulbecco's modified Eagle's medium (DMEM; catalog no. 10013, Corning) supplemented with 10% fetal bovine serum (FBS; catalog no. F2442, Sigma-Aldrich) and 1% penicillin-streptomycin-glutamine (catalog no. 10378016, Gibco). T cell culture medium (denoted as C10 medium) was made of RPMI 1640 (catalog no. 10040, Corning) supplemented with 10% FBS (catalog no. F2442, Sigma-Aldrich), 1% penicillin-streptomycin-glutamine (catalog no. 10378016, Gibco), 0.2% Normocin (catalog no. ant-nr-2, InvivoGen), 1% Minimal Essential Medium (MEM) Non-essential Amino Acid Solution (catalog no. 11140050, Gibco), 1% HEPES (catalog no. 15630080, Gibco), 1% sodium pyruvate (catalog no. 11360070, Gibco), and 0.05 mM β-mercaptoethanol (catalog no. M3148, Sigma-Aldrich).

Cell culture reagents—including purified no azide/low endotoxin (NA/LE) anti-mouse CD3ε (catalog no. 553057, clone 145-2C11), purified NA/LE anti-mouse CD28 (catalog no. 553294, clone 37.51), anti-human CD3 (catalog no. 56685, clone OKT3), and anti-human CD28 (catalog no. 555725, clone CD28.2)—were purchased form BD Biosciences. Recombinant human IL-2 (catalog no. 200-02) was purchased from PeproTech.

In vivo depletion antibodies, including anti-mouse CD8α (catalog no. BE0061, clone RMP2.43) and its isotype control [rat immunoglobulin G2b (IgG2b), catalog no. BE0090], were purchased from BioXCell. In vivo PD-1–blocking antibody (catalog no. BE0146, clone RMP1-14) and its isotype control (rat IgG2a, catalog no. BE0089) were purchased from BioXCell.

MAOIs—including phenelzine (catalog no. P6777), moclobemide (catalog no. M3071), and clorgyline (catalog no. M3778)—were purchased from Sigma-Aldrich. Serotonin (catalog no. H9532) and serotonin receptor (5-HTR) antagonist asenapine (catalog no. A7861) were also purchased from Sigma-Aldrich.

Syngeneic mouse tumor models

B16-OVA melanoma cells (1×10^6 per animal) or MC38 colon cancer cells (3×10^5 per animal) were subcutaneously injected into experimental mice to form solid tumors. In some experiments, mice received intraperitoneal injection of MAOIs [i.e., phenelzine (30 mg/kg per day), moclobemide (50 mg/kg per day), or clorgyline (50 mg/kg per day)] to block MAO-A activity. In some experiments, mice received intraperitoneal injection of anti-mouse CD8α antibodies (200 μg per animal, twice per week) to deplete CD8 T cells; mice that received intraperitoneal injection of isotype antibodies were included as controls. In some experiments, mice received intraperitoneal injection of anti-mouse PD-1 antibodies (300 μg per animal, twice per week) to block PD-1; mice that received intraperitoneal injection of isotype antibodies were included as controls.

During an experiment, tumor growth was monitored twice per week by measuring tumor size using a Fisherbrand Traceable digital caliper (Thermo Fisher Scientific); tumor volumes were calculated by formula $1/2 \times L \times W^2$. At the end of an experiment, TIIs were isolated for analysis using qPCR, flow cytometry, and/or scRNA-seq. In some experiments, sera were also collected for serotonin measurement.

Two-way BM transfer B16-OVA tumor model

BM cells were collected from femurs and tibias of donor mice and were transferred into the recipient mice through retro-orbital (r.o.) injection. Recipient mice were preconditioned with whole-body irradiation (1200 gray). For BM transfer experiments confining MAO-A deficiency comparison to immune cells, *Maoa*-WT or *Maoa*-KO BM cells were transferred into CD45.1 recipient mice (8 to 10×10^6 cells per recipient mouse). For BM transfer experiments confining MAO-A deficiency comparison to nonimmune cells, WT CD45.1 BM cells were transferred into *Maoa*-WT or *Maoa*-KO recipient mice (8 to 10×10^6 cells per recipient mouse). After BM transfer, recipient mice were maintained on antibiotic water (Amoxil; 0.25 mg/ml) for 4 weeks. Periodic bleedings were performed to monitor immune cell reconstitution using flow cytometry. At 8 to 12 weeks after BM transfer, recipient mice were fully immune-reconstituted and were used for tumor challenge experiments. B16-OVA mouse melanoma cells were subcutaneously injected into experimental mice to form solid tumors (1×10^6 cells per animal). Tumor growth was monitored twice per week by measuring tumor size using a Fisherbrand Traceable digital caliper; tumor volumes were calculated by formula $1/2 \times L \times W^2$.

Adoptive OT1 T cell transfer B16-OVA tumor model

Spleen and lymph node cells were harvested from the *OT1*-Tg or *OT1*-Tg/*Maoa*-KO mice and were subjected to magnetic-activated cell sorting (MACS) using the Mouse CD8 T Cell Isolation Kit (catalog no. 120117044, Miltenyi Biotec) following the manufacturer's instructions. The purified OT1 T cells (identified as $CD8^+TCR\ V\beta5^+$ cells) were adoptively transferred to tumor-bearing CD45.1 wild-type mice (1×10^5 cells per recipient mouse). CD45.1 mice were subcutaneously inoculated with B16-OVA tumor cells 1 week in advance (1×10^6 cells per animal). Before OT1 T cell adoptive transfer, recipient mice were preconditioned with whole-body irradiation (600 gray). During an experiment, tumor growth was monitored twice per week by measuring tumor size using a Fisherbrand Traceable digital caliper; tumor volumes were calculated by formula $1/2 \times L \times W^2$. Mice were terminated at the indicated time points, and TIIs were isolated for flow cytometry analysis of surface marker expression and intracellular effector molecule production.

Xenograft human tumor model

The A375-A2-ESO-FG human melanoma cells (10×10^6 cells per animal) were subcutaneously injected into NSG mice to form solid tumors. In some experiments, mice received phenelzine treatment through intraperitoneal injection (30 mg/kg per day). In some experiments, mice received adoptive transfer of ESO-T cells through retro-orbital injection (4×10^6 cells per recipient mouse). Before ESO-T cell adoptive transfer, recipient mice were preconditioned with total body irradiation (100 gray). During an experiment, tumor growth was monitored twice per week by measuring tumor size using a Fisherbrand Traceable digital caliper; tumor volumes were calculated by formula $1/2 \times L \times W^2$.

TII isolation and analysis

Solid tumors were harvested from experimental mice and mechanically disrupted through 70-μm nylon mesh strainers to release single cells (catalog no. 07-201-431, Corning). Single cells were washed once with C10 medium, resuspended in 50% Percoll (catalog no. P4937, Sigma-Aldrich), and centrifuged at 800*g* at 25°C for 30 min with brake off. Cell pellets enriched with TIIs were then collected and resuspended in C10 medium for further analysis.

In the experiments studying the *Maoa* gene expression in TIIs, day 14 B16-OVA tumors were harvested from B6 wild-type mice to prepare TII suspensions. TII suspensions were then sorted using a FACSAria II flow cytometer (BD Biosciences) to purify immune cells (gated as $DAPI^-CD45.2^+$ cells), which were then subjected to qPCR analysis of *Maoa* mRNA expression.

In the experiments studying the *Maoa* gene expression in tumor-infiltrating CD8 T cell subsets, day 14 B16-OVA tumors were harvested from B6 wild-type mice to prepare TII suspensions. Tumor-infiltrating CD8 T cells (pregated as $CD45.2^+TCR\beta^+CD8^+$ cells) were sorted into three subsets (gated as $PD\text{-}1^{lo}$, $PD\text{-}1^{hi}Tim\text{-}3^{lo}LAG\text{-}3^{lo}$, and $PD\text{-}1^{hi}Tim\text{-}3^{hi}LAG\text{-}3^{hi}$ cells) using a FACSAria II flow cytometer and then were subjected to qPCR analysis of *Maoa* mRNA expression.

In the experiments studying gene expression profiling of TIIs, day 14 B16-OVA tumors were harvested from *Maoa*-WT and *Maoa*-KO mice to prepare TII suspensions. TII suspensions were then sorted using a FACSAria II flow cytometer to purify immune cells (gated as $DAPI^-CD45.2^+$ cells), which were then subjected to scRNA-seq analysis.

In other experiments, TII suspensions prepared under indicated experimental conditions were directly analyzed by flow cytometry to study surface marker expression and intracellular effector molecule production of CD8 T cells (pregated as $CD45.2^+TCR\beta^+CD8^+$ cells).

In vitro mouse CD8 T cell culture

Spleen and lymph node cells were harvested from *Maoa*-KO or *Maoa*-WT (B6 wild-type) mice and subjected to MACS using the Mouse CD8 T Cell Isolation Kit (catalog no. 120117044, Miltenyi Biotec) following the manufacturer's instructions. Purified mouse CD8 T cells were cultured in vitro in C10 medium, in a 24-well plate at 0.5×10^6 cells/ml medium per well, in the presence of plate-bound anti-mouse CD3ε (5 μg/ml) for up to 4 days. At indicated time points, cells were collected for flow cytometry analysis of surface marker expression and intracellular effector molecule production and for qPCR analysis of mRNA expression; cell culture supernatants were collected for ELISA analysis of effector cytokine production.

In experiments studying serotonin signaling, cells were cultured in C10 medium made of serotonin-depleted FBS that was pretreated overnight with charcoal-dextran (1 g per 50 ml of FBS; catalog no. C6241, Sigma-Aldrich). L-Ascorbic acid (100 μM; catalog no. A4403, Sigma-Aldrich) was added to C10 medium to stabilize T cell–produced or –supplemented serotonin. In some experiments, cells were treated with MAOIs to block MAO-A activity; MAOIs studied were phenelzine (10 μM), moclobemide (200 μM), or clorgyline (20 μM). In some experiments, cells were supplemented with exogenous serotonin (10 μM) to stimulate serotonin signaling. In some experiments, cells were treated with serotonin receptor antagonist asenapine (10 μM) to block serotonin receptor signaling.

In vitro human CD8 T cell culture

Healthy donor human peripheral blood mononuclear cells (PBMCs) were purchased from the UCLA Center for AIDS Research (CFAR) Virology Core Laboratory. PBMCs were cultured in C10 medium in the presence of plate-bound anti-human CD3 (1 μg/ml) and soluble anti-human CD28 (1 μg/ml). After 5 days, activated CD8 T cells were sorted out on the basis of surface markers ($CD45^+TCR\alpha\beta^+CD8^+$) using a FACSAria II flow cytometer (BD Biosciences). Naïve CD8 T cells were sorted from the same donors based on surface markers ($CD45^+TCR\alpha\beta^+CD8^+CD62L^{hi}CD45RO^{low}$) and were included as controls. The purified naïve and effector human CD8 T cells were then analyzed for *MAOA* mRNA expression using qPCR.

In vitro OT1 T cell culture

Spleen and lymph node cells were harvested from the *OT1*-Tg or *OT1*-Tg/*Maoa*-KO mice and then subjected to MACS sorting using the Mouse CD8 T Cell Isolation Kit (catalog no. 120117044, Miltenyi Biotec) following the manufacturer's instructions. The purified OT1 T cells (identified as $CD8^+TCR\ V\beta5^+$ cells) were cultured in C10 medium, in a 24-well plate at 0.5×10^6 cells per ml medium per well, in the presence of plate-bound anti-mouse CD3ε (5 μg/ml) for up to 4 days. At the indicated time points, cells were collected for flow cytometry analysis of surface marker expression; cell culture supernatants were collected for ELISA analysis of effector cytokine production.

MIG-Maoa retroviral vector and mouse CD8 T cell transduction

The MIG-*Maoa* retroviral vector was constructed by inserting a codon-optimized *Maoa* complementary DNA (cDNA) [synthesized by Integrated DNA Technologies (IDT)] into the parental MIG retroviral vector (*45*). The vesicular stomatitis virus glycoprotein (VSVG)–pseudotyped MIG and MIG-*Maoa* retroviruses were produced using 293T virus–packaging cells following a standard calcium precipitation method (*46*, *47*) and then were used to transduce Phoenix-ECO cells to generate stable cell lines producing ECO-pseudotyped MIG or MIG-*Maoa* retroviruses (denoted as Phoenix-ECO-MIG and Phoenix-ECO-MIG-*Maoa* cell lines, respectively). For virus production, Phoenix-ECO-MIG and Phoenix-ECO-MIG-*Maoa* cells were seeded at a density of 0.8×10^6 cells/ml in D10 medium and cultured in a 15-cm dish (30 ml per dish) for 2 days; virus supernatants were then harvested and freshly used for spin infection.

MACS-purified CD8 T cells isolated from the *Maoa*-KO mice were cultured in vitro and stimulated with plate-bound anti-mouse CD3ε (5 μg/ml) for 4 days. On days 2 and 3, cells were spin-infected with ECO-pseudotyped MIG or MIG-*Maoa* retroviral supernatants supplemented with polybrene (10 μg/ml; catalog no. TR-1003-G, Millipore) at 1321*g* at 30°C for 90 min. On day 4, cells were collected for flow cytometry analysis of transduction efficiency and for qPCR analysis of effector gene expression.

Retro/ESO-TCR retroviral vector and human CD8 T cell transduction

The Retro/ESO-TCR vector was constructed by inserting into the parental pMSGV vector a synthetic gene encoding an HLA-A2–restricted, NY-ESO-1 tumor antigen-specific human CD8 TCR (clone 3A1) (*24*). VSVG-pseudotyped Retro/ESO-TCR retroviruses were generated by transfecting 293T cells following a standard calcium precipitation protocol and an ultracentrifugation concentration protocol (*48*); the viruses were then used to transduce PG13 cells to generate a stable retroviral packaging cell line producing gibbon ape leukemia virus (GaLV) glycoprotein-pseudotyped Retro/ESO-TCR retroviruses (denoted as PG13-ESO-TCR cell line). For virus production, the PG13-ESO-TCR cells were seeded at a density of 0.8×10^6 cells/ml in D10 medium and cultured in a 15-cm dish (30 ml per dish) for 2 days; virus supernatants were then harvested and stored at −80°C for future use.

Healthy donor PBMCs were stimulated with plate-bound anti-human CD3 (1 μg/ml) and soluble anti-human CD28 (1 μg/ml) in the presence of recombinant human IL-2 (300 U/ml). On day 2, cells were spin-infected with frozen-thawed Retro/ESO-TCR retroviral supernatants supplemented with polybrene (10 μg/ml) at 660*g* at 30°C for 90 min after an established protocol (*25*). Transduced human CD8 T cells (denoted as ESO-T cells) were expanded for another 7 to 10 days and then cryopreserved for future use. Mock-transduced human CD8 T cells (denoted as Mock-T cells) were generated as controls.

In vitro A375-A2-ESO-FG human melanoma cell-killing assay

The A375-A2-ESO-FG human melanoma cells (5 to 10×10^3 cells per well) were cocultured with either ESO-T cells or Mock-T cells at indicated ratios in C10 medium in a Corning 96-well clear bottom black plate (catalog no. 3603, Corning). At 24 hours, live tumor cells were quantified by adding D-luciferin (150 μg/ml; part no. 119222, Caliper Life Science) to cell cultures and reading out luciferase activities using an Infinite M1000 microplate reader (Tecan) according to the manufacturer's instructions.

Flow cytometry (FACS)

Flow cytometry, also known as fluorescence-activated cell sorting (FACS), was used to analyze surface marker and intracellular effector molecule expression of T cells. Fluorochrome-conjugated monoclonal antibodies specific for mouse CD45.2 (clone 104), TCRβ

(clone H57-597), CD4 (clone RM4-5), CD8 (clone 53-6.7), CD69 (clone H1.2F3), CD25 (clone PC61), CD44 (clone IM7), CD62L (clone MEL-14), and IFN-γ (clone XMG1.2) were purchased from BioLegend. Monoclonal antibodies specific for mouse tumor necrosis factor–α (TNF-α; clone JES6-5H4) and Fc block (anti-mouse CD16/32) (clone 2.4G2) were purchased from BD Biosciences. Monoclonal antibodies specific for mouse PD-1 (clone RMP1-30) was purchased from Thermo Fisher Scientific. Fluorochrome-conjugated monoclonal antibodies specific for human CD45 (clone H130), TCRαβ (clone I26), CD4 (clone OKT4), CD8 (clone SK1), CD45RO (clone UCHL1), CD62L (clone DREG-56), and human Fc receptor–blocking solution (TruStain FcX, catalog no. 422302) were purchased from BioLegend. Fixable Viability Dye eFluor 506 (catalog no. 65-0866) was purchased from Thermo Fisher Scientific. OVA dextramer (catalog no. JD2163) was purchased from Immudex.

To study T cell surface marker expression, cells were stained with Fixable Viability Dye first, followed by Fc blocking and surface marker staining, according to a standard procedure as described previously (*47*). To study T cell intracellular cytokine production, CD8 T cells or primary TIIs were stimulated with phorbol-12-myristate-13-acetate (PMA) (50 ng/ml; catalog no. 80055-400, VWR) and ionomycin (500 ng/ml; catalog no. 80056-892, VWR) in the presence of GolgiStop (4 μl per 6-ml culture; catalog no. 554724, BD Biosciences) for 4 hours. At the end of the culture, cells were collected, and intracellular cytokine (i.e., IFN-γ and TNF-α) staining was performed using the Fixation/Permeabilization Solution Kit (catalog no. 554714, BD Biosciences) and following the manufacturer's instructions. To study T cell intracellular cytotoxicity molecule production, CD8 T cells or primary TIIs were collected and then directly subjected to intracellular Granzyme B staining using the Fixation/Permeabilization Solution Kit (BD Biosciences). These cells were costained with surface markers to identify CD8 T cells (gated as $TCR\beta^+CD8^+$ cells in vitro or $CD45.2^+TCR\beta^+CD8^+$ cells in vivo) or OT1 cells (gated as $CD45.2^+CD8^+$ cells in vivo). Stained cells were analyzed by using a MACSQuant Analyzer 10 flow cytometer (Miltenyi Biotec). A FlowJo software (Tree Star) was used to analyze the data.

Enzyme-linked immunosorbent assay (ELISA)

To study T cell cytokine production, MACS-purified mouse CD8 T cells were cultured in C10 medium under indicated experimental conditions for up to 4 days. At indicated time points, cell culture supernatants were collected for cytokine ELISA analysis following a standard protocol from the BD Biosciences. The coating and biotinylated antibodies for the detection of mouse IFN-γ (coating antibody, catalog no. 554424; biotinylated detection antibody, catalog no. 554426) and IL-2 (coating antibody, catalog no. 551216; biotinylated detection antibody, catalog no. 554410) were purchased from BD Biosciences. The streptavidin–horseradish peroxidase (HRP) conjugate (catalog no. 18410051) was purchased from Invitrogen. Mouse IFN-γ (catalog no. 575309) and IL-2 (catalog no. 575409) standards were purchased from BioLegend. The 3,3′,5,5′-tetramethylbenzidine (TMB; catalog no. 51200048) substrate was purchased from Kirkegaard & Perry Laboratories (KPL). The absorbance at 450 nm was measured using an Infinite M1000 microplate reader (Tecan).

To study T cell serotonin production, MACS-purified mouse CD8 T cells were cultured in C10 medium made of serotonin-depleted FBS and supplemented with L-ascorbic acid, in the presence of plate-bound anti-mouse CD3ε (5 μg/ml) for up to 4 days. At indicated time points, cell culture supernatants were collected for serotonin ELISA analysis using a commercial kit following the manufacturer's instructions (SEU39-K01, Eagle Biosciences). The absorbance at 450 nm was measured using an Infinite M1000 microplate reader (Tecan).

Western blots

CD8 T cells purified from *Maoa*-WT and *Maoa*-KO mice were cultured in vitro in a 24-well plate at 0.5×10^6 cells per well for 2 days, in the presence of plate-bound anti-mouse CD3ε (5 μg/ml), with or without asenapine treatment (10 μM). Cells were then rested on ice for 2 hours and restimulated with plate-bound anti-mouse CD3ε (5 μg/ml) for 20 min. Total protein was extracted using a lysis buffer containing 20 mM HEPES (pH 7.6), 150 mM NaCl, 1 mM EDTA, 1% TritonX-100, and protease/phosphatase inhibitor cocktail (catalog no. 5872S, Cell Signaling Technology). Nuclear protein was extracted using the Nuclear Protein Extraction Kit (catalog no. P178833, Thermo Fisher Scientific). Protein concentration was measured using the Bicinchoninic Acid (BCA) Assay Kit (catalog nos. 23228 and 1859078, Thermo Fisher Scientific). Equal amounts of protein were resolved on a 10% SDS–polyacrylamide gel electrophoresis gel and then transferred to a polyvinylidene difluoride (PVDF) membrane by electrophoresis. MAO-A antibody was purchased from Abcam (catalog no. ab126751, clone EPR7101). The following antibodies were purchased from the Cell Signaling Technology and used to blot for the proteins of interest: anti-mouse NF-κB p65 (catalog no. 8242P, clone D14E12), anti-mouse c-Jun (catalog no. 9165S, clone 60A8), anti-mouse NFAT (catalog no. 4389S), anti-mouse ERK1/2 (catalog no. 9107S, clone 3A7), anti-mouse p-ERK1/2 (catalog no. 4370S, clone D13.14.4E), secondary anti-mouse (catalog no. 7076P2), and secondary anti-rabbit (catalog no. 7074P2). β-Actin (catalog no. sc-69879, clone AC-15, Santa Cruz Biotechnology) was used as an internal control for total protein extracts, whereas Lamin A/C (catalog no. 39287, clone 3A6-4C11, Active Motif) was used as an internal control for nuclear protein extracts. Signals were visualized with autoradiography using an enhanced chemiluminesence (ECL) system (catalog no. RPN2232, Thermo Fisher Scientific). The data were analyzed using an Image Lab software (Bio-Rad).

High-performance liquid chromatography (HPLC)

HPLC was used to measure intratumoral and serum serotonin levels as previously described (*49*, *50*). Briefly, tumors and sera were collected from experimental mice at indicated time points and were snap-frozen using liquid nitrogen. Frozen samples were thawed and homogenized using methanol and acetonitrile by vortexing. Homogenized samples were centrifuged, and supernatants were collected to new tubes and evaporated under a stream of argon. Dried sample pellets were then reconstituted in HPLC running buffer and were ready for analysis. Serotonin concentration was quantified using a C18 column by reverse-phase HPLC (System Gold 166P detector, Beckman Coulter). For tumor samples, both intracellular and interstitial serotonin were analyzed.

mRNA quantitative RT-PCR (mRNA qPCR)

Total RNA was isolated using TRIzol reagent (catalog no. 15596018, Invitrogen, Thermo Fisher Scientific) according to the manufacturer's instructions. cDNA was prepared using the SuperScript III First-Strand Synthesis SuperMix Kit (catalog no. 18080400, Invitrogen,

Thermo Fisher Scientific). Gene expression was measured using the KAPA SYBR FAST qPCR Kit (catalog no. KM4117, Kapa Biosystems) and the 7500 Real-time PCR System (Applied Biosystems) according to the manufacturer's instructions. *Ube2d2* was used as an internal control for mouse immune cells, and *ACTIN* was used as an internal control for human immune cells. The relative expression of the mRNA of interest was calculated using the $2^{\Delta\Delta CT}$ method. Primer sequences are available in table S1.

Single-cell RNA sequencing (scRNA-seq)

scRNA-seq was used to analyze the gene expression profiling of TIIs. Day 14 B16-OVA tumors were harvested from *Maoa*-WT and *Maoa*-KO mice to prepare TII suspensions (10 tumors were combined for each group). TII suspensions were then sorted using a FACSAria II flow cytometer to purify immune cells (gated as $DAPI^{-}CD45.2^{+}$ cells). Sorted TIIs were immediately delivered to the Technology Center for Genomics & Bioinformatics (TCGB) facility at UCLA for library construction and sequencing. Briefly, purified TIIs were quantified using a Cell Countess II automated cell counter (Invitrogen/Thermo Fisher Scientific). A total of 10,000 TIIs from each experimental group were loaded on the Chromium platform (10x Genomics), and libraries were constructed using the Chromium Single Cell 3′ Library & Gel Bead Kit v2 (catalog no. PN-120237, 10x Genomics) according to the manufacturer's instructions. Libraries were sequenced on an Illumina NovaSeq using the NovaSeq 6000 S2 Reagent Kit (100 cycles; 20012862, Illumina). Data analysis was performed using a Cell Ranger Software Suite (10x Genomics). Binary base call (BCL) files were extracted from the sequencer and used as inputs for the Cell Ranger pipeline to generate the digital expression matrix for each sample. Then, cellranger aggr command was used to aggregate the two samples into one digital expression matrix. The matrix was analyzed using Seurat, an R package designed for scRNA-seq. Specifically, cells were first filtered to have at least 300 unique molecular identifiers (UMIs), at least 100 genes, and at most 50% mitochondrial gene expression; only one cell did not pass the filter. The filtered matrix was normalized using the Seurat function NormalizeData. Variable genes were found using the Seurat function FindVariableGenes. The matrix was scaled to regress out the sequencing depth for each cell. Variable genes that had been previously identified were used in principal components analysis (PCA) to reduce the dimensions of the data. After this, 13 principal components (PCs) were used in Uniform Manifold Approximation and Projection (UMAP) to further reduce the dimensions to two. The same 13 PCs were also used to group the cells into different clusters by the Seurat function FindClusters. Next, marker genes were found for each cluster and used to define the cell types. Subsequently, three clusters of antigen-experienced tumor-infiltrating CD8 T cells (identified by coexpression of *Cd8a*, *Cd3d*, and *Cd44* marker genes) were extracted and compared between the *Maoa*-WT and *Maoa*-KO samples.

For GSEA, signal-to-noise ratio was used to rank the genes in correlation with indicated gene signatures. For each cluster, the average expression of each gene in this cluster and in all other clusters was calculated. Fold changes were calculated by comparing the average expressions. The genes were then ranked by fold changes from high to low. To compare our data to preannotated datasets, we used the CD8 T cell subtype marker genes published by Miller *et al.* (*16*). GSEA was performed on these marker genes against the ranked genes in our dataset.

Tumor Immune Dysfunction and Exclusion (TIDE) computational method

TIDE analysis was performed as previously described (*26*, *51*) (http://tide.dfci.harvard.edu/query/). Briefly, this method was used to study the association between the tumor-infiltrating CD8 T cell [also known as cytotoxic T lymphocyte (CTL)] level and overall patient survival in relation to the intratumoral *MAOA* gene expression level. For each patient cohort, tumor samples were divided into *MAOA*-high (samples with *MAOA* expression one standard derivation above the average) and *MAOA*-low (remaining samples) groups, followed by analyzing the association between the CTL levels and survival outcomes in each group. The CTL level was estimated as the average expression level of *CD8A*, *CD8B*, *GZMA*, *GZMB*, and *PRF1*. Each survival plot presented tumors in two subgroups: "CTL-high" group had above-average CTL values among all samples, whereas "CTL-low" group had below-average CTL values. A T cell dysfunction score (*z* score) was calculated for each patient cohort, correlating the *MAOA* expression level with the beneficial effect of CTL infiltration on patient survival. A positive *z* score indicates that the expression of *MAOA* is negatively correlated with the beneficial effect of tumor-infiltrating CTL on patient survival. The *P* value indicates the comparison between the *MAOA*-low and *MAOA*-high groups and was calculated by two-sided Wald test in a Cox proportional hazards (Cox-PH) regression.

Statistics

A GraphPad Prism 7 software (GraphPad Software) was used for the graphic representation and statistical analysis of the data. Pairwise comparisons were made using a two-tailed Student's *t* test. Multiple comparisons were performed using an ordinary one-way analysis of variance (ANOVA) followed by Tukey's multiple comparisons test or a two-way repeated measures ANOVA followed by Sidak multiple comparisons test. Data are presented as the means ± SEM, unless otherwise indicated. A *P* value of less than 0.05 was considered significant. ns, not significant; $*P < 0.05$, $**P < 0.01$, and $***P < 0.001$. The *P* values of violin plots were determined by Wilcoxon rank sum test. The *P* values of comparison between survival plots were calculated by testing the association between TIDE prediction scores and overall survival with the two-sided Wald test in a Cox-PH regression.

SUPPLEMENTARY MATERIALS

immunology.sciencemag.org/cgi/content/full/6/59/eabh2383/DC1

Fig. S1. Characterization of *Maoa*-KO mice (related to Fig. 1).

Fig. S2. MAO-A–deficient mice show suppressed tumor growth and enhanced CD8 T cell antitumor immunity (related to Fig. 1, E to M).

Fig. S3. MAO-A–deficient tumor-infiltrating CD8 T cells show enhanced mitochondrial electron transport chain gene expression (related to Fig. 1, K to M).

Fig. S4. MAO-A directly regulates antitumor immunity (related to Fig. 2, A to C).

Fig. S5. MAO-A directly regulates CD8 T cell antitumor immunity (related to Fig. 2, D to F).

Fig. S6. MAO-A acts as a negative-feedback regulator to restrain CD8 T cell activation (related to Fig. 3).

Fig. S7. MAO-A acts as a negative-feedback regulator to restrain CD8 T cell activation: Studying antigen-specific T cells (related to Fig. 3).

Fig. S8. MAO-A regulates CD8 T cell autocrine serotonin signaling (related to Fig. 4).

Fig. S9. MAOI treatment induces CD8 T cell hyperactivation in vitro (related to Fig. 5A).

Fig. S10. MAO-A blockade for cancer immunotherapy: Syngeneic mouse tumor model studies (related to Fig. 5).

Fig. S11. MAO-A blockade for cancer immunotherapy: Immunodeficient NSG mouse tumor model studies (related to Fig. 5).

Fig. S12. MAO-A blockade for cancer immunotherapy: Human T cell studies (related to Fig. 6, A to D).

Fig. S13. Clinical data correlation studies identify MAO-A as a negative regulator of T cell antitumor function in patients with cancer (related to Fig. 6, E and F).

Fig. S14. The intratumoral MAO-A–serotonin axis model.
Table S1. Primer sequences for qPCR.
Table S2. Raw data file (Excel spreadsheet).
Reproducibility checklist

View/request a protocol for this paper from *Bio-protocol*.

REFERENCES AND NOTES

1. J. Couzin-Frankel, Breakthrough of the year 2013. Cancer immunotherapy. *Science* **342**, 1432–1433 (2013).
2. S. A. Rosenberg, N. P. Restifo, Adoptive cell transfer as personalized immunotherapy for human cancer. *Science* **348**, 62–68 (2015).
3. W. A. Lim, C. H. June, The principles of engineering immune cells to treat cancer. *Cell* **168**, 724–740 (2017).
4. S. H. Baumeister, G. J. Freeman, G. Dranoff, A. H. Sharpe, Coinhibitory pathways in immunotherapy for cancer. *Annu. Rev. Immunol.* **34**, 539–573 (2016).
5. D. B. Page, M. A. Postow, M. K. Callahan, J. P. Allison, J. D. Wolchok, Immune modulation in cancer with antibodies. *Annu. Rev. Med.* **65**, 185–202 (2014).
6. A. Ribas, Releasing the brakes on cancer immunotherapy. *N. Engl. J. Med.* **373**, 1490–1492 (2015).
7. M. Dougan, G. Dranoff, S. K. Dougan, Cancer immunotherapy: Beyond checkpoint blockade. *Annu. Rev. Cancer Biol.* **3**, 55–75 (2019).
8. J. C. Shih, K. Chen, M. J. Ridd, Monoamine oxidase: From genes to behavior. *Annu. Rev. Neurosci.* **22**, 197–217 (1999).
9. J. E. Pintar, X. O. Breakefield, Monoamine oxidase (MAO) activity as a determinant in human neurophysiology. *Behav. Genet.* **12**, 53–68 (1982).
10. H. G. Brunner, M. Nelen, X. O. Breakefield, H. H. Ropers, B. A. van Oost, Abnormal behavior associated with a point mutation in the structural gene for monoamine oxidase A. *Science* **262**, 578–580 (1993).
11. J. H. Meyer, N. Ginovart, A. Boovariwala, S. Sagrati, D. Hussey, A. Garcia, T. Young, N. Praschak-Rieder, A. A. Wilson, S. Houle, Elevated monoamine oxidase a levels in the brain: an explanation for the monoamine imbalance of major depression. *Arch. Gen. Psychiatry* **63**, 1209–1216 (2006).
12. J. Tiihonen, M. R. Rautiainen, H. M. Ollila, E. Repo-Tiihonen, M. Virkkunen, A. Palotie, O. Pietiläinen, K. Kristiansson, M. Joukamaa, H. Lauerma, J. Saarela, S. Tyni, H. Vartiainen, J. Paananen, D. Goldman, T. Paunio, Genetic background of extreme violent behavior. *Mol. Psychiatry* **20**, 786–792 (2015).
13. A. Gibbons, American Association of Physical Anthropologists meeting. Tracking the evolutionary history of a "warrior" gene. *Science* **304**, 818 (2004).
14. M. Bortolato, K. Chen, J. C. Shih, Monoamine oxidase inactivation: From pathophysiology to therapeutics. *Adv. Drug Deliv. Rev.* **60**, 1527–1533 (2008).
15. M. Bortolato, K. Chen, S. C. Godar, G. Chen, W. Wu, I. Rebrin, M. R. Farrell, A. L. Scott, C. L. Wellman, J. C. Shih, Social deficits and perseverative behaviors, but not overt aggression, in MAO-A hypomorphic mice. *Neuropsychopharmacology* **36**, 2674–2688 (2011).
16. B. C. Miller, D. R. Sen, R. Al Abosy, K. Bi, Y. V. Virkud, M. W. LaFleur, K. B. Yates, A. Lako, K. Felt, G. S. Naik, M. Manos, E. Gjini, J. R. Kuchroo, J. J. Ishizuka, J. L. Collier, G. K. Griffin, S. Maleri, D. E. Comstock, S. A. Weiss, F. D. Brown, A. Panda, M. D. Zimmer, R. T. Manguso, F. S. Hodi, S. J. Rodig, A. H. Sharpe, W. N. Haining, Subsets of exhausted $CD8^+$ T cells differentially mediate tumor control and respond to checkpoint blockade. *Nat. Immunol.* **20**, 326–336 (2019).
17. F. Malinarich, K. Duan, R. A. Hamid, A. Bijin, W. X. Lin, M. Poidinger, A. M. Fairhurst, J. E. Connolly, High mitochondrial respiration and glycolytic capacity represent a metabolic phenotype of human tolerogenic dendritic cells. *J. Immunol.* **194**, 5174–5186 (2015).
18. L. T. Nguyen, P. S. Ohashi, Clinical blockade of PD1 and LAG3–potential mechanisms of action. *Nat. Rev. Immunol.* **15**, 45–56 (2015).
19. E. J. Wherry, M. Kurachi, Molecular and cellular insights into T cell exhaustion. *Nat. Rev. Immunol.* **15**, 486–499 (2015).
20. Y. Chen, M. Leon-Ponte, S. C. Pingle, P. J. O'Connell, G. P. Ahern, T lymphocytes possess the machinery for 5-HT synthesis, storage, degradation and release. *Acta Physiol (Oxf.)* **213**, 860–867 (2015).
21. M. León-Ponte, G. P. Ahern, P. J. O'Connell, Serotonin provides an accessory signal to enhance T-cell activation by signaling through the 5-HT_7 receptor. *Blood* **109**, 3139–3146 (2007).
22. P. J. O'Connell, X. Wang, M. Leon-Ponte, C. Griffiths, S. C. Pingle, G. P. Ahern, A novel form of immune signaling revealed by transmission of the inflammatory mediator serotonin between dendritic cells and T cells. *Blood* **107**, 1010–1017 (2006).
23. M. Wimbiscus, O. Kostenko, D. Malone, MAO inhibitors: Risks, benefits, and lore. *Cleve. Clin. J. Med.* **77**, 859–882 (2010).
24. M. T. Bethune, X. H. Li, J. Yu, J. McLaughlin, D. Cheng, C. Mathis, B. H. Moreno, K. Woods, A. J. Knights, A. Garcia-Diaz, S. Wong, S. Hu-Lieskovan, C. Puig-Saus, J. Cebon, A. Ribas, L. Yang, O. N. Witte, D. Baltimore, Isolation and characterization of NY-ESO-1-specific T cell receptors restricted on various MHC molecules. *Proc. Natl. Acad. Sci. U.S.A.* **115**, E10702–E10711 (2018).
25. Y. Zhu, D. J. Smith, Y. Zhou, Y.-R. Li, J. Yu, D. Lee, Y.-C. Wang, S. D. Biase, X. Wang, C. Hardoy, J. Ku, T. Tsao, L. J. Lin, A. T. Pham, H. Moon, J. M. Laughlin, D. Cheng, R. P. Hollis, B. Campo-Fernandez, F. Urbinati, L. Wei, L. Pang, V. Rezek, B. Berent-Maoz, M. H. Macabali, D. Gjertson, X. Wang, Z. Galic, S. G. Kitchen, D. S. An, S. Hu-Lieskovan, P. J. Kaplan-Lefko, S. N. De Oliveira, C. S. Seet, S. M. Larson, S. J. Forman, J. R. Heath, J. A. Zack, G. M. Crooks, C. G. Radu, A. Ribas, D. B. Kohn, O. N. Witte, L. Yang, Development of hematopoietic stem cell-engineered invariant natural killer T cell therapy for cancer. *Cell Stem Cell* **25**, 542–557 (2019).
26. P. Jiang, S. Gu, D. Pan, J. Fu, A. Sahu, X. Hu, Z. Li, N. Traugh, X. Bu, B. Li, J. Liu, G. J. Freeman, M. A. Brown, K. W. Wucherpfennig, X. S. Liu, Signatures of T cell dysfunction and exclusion predict cancer immunotherapy response. *Nat. Med.* **24**, 1550–1558 (2018).
27. D.-T. Chen, J. M. Hernandez, D. Shibata, S. M. McCarthy, L. A. Humphries, W. Clark, A. Elahi, M. Gruidl, D. Coppola, T. Yeatman, Complementary strand microRNAs mediate acquisition of metastatic potential in colonic adenocarcinoma. *J. Gastrointest. Surg.* **16**, 905–912 (2012).
28. S. Rousseaux, A. Debernardi, B. Jacquiau, A.-L. Vitte, A. Vesin, H. Nagy-Mignotte, D. Moro-Sibilot, P.-Y. Brichon, S. Lantuejoul, P. Hainaut, J. Laffaire, A. de Reyniès, D. G. Beer, J.-F. Timsit, C. Brambilla, E. Brambilla, S. Khochbin, Ectopic activation of germline and placental genes identifies aggressive metastasis-prone lung cancers. *Sci. Transl. Med.* **5**, 186ra66 (2013).
29. Cancer Genome Atlas Research Network, J. N. Weinstein, E. A. Collisson, G. B. Mills, K. R. M. Shaw, B. A. Ozenberger, K. Ellrott, I. Shmulevich, C. Sander, J. M. Stuart, The Cancer Genome Atlas Pan-Cancer analysis project. *Nat. Genet.* **45**, 1113–1120 (2013).
30. J. K. Stratford, D. J. Bentrem, J. M. Anderson, C. Fan, K. A. Volmar, J. S. Marron, E. D. Routh, L. S. Caskey, J. C. Samuel, C. J. der, L. B. Thorne, B. F. Calvo, H. J. Kim, M. S. Talamonti, C. A. Iacobuzio-Donahue, M. A. Hollingsworth, C. M. Perou, J. J. Yeh, A six-gene signature predicts survival of patients with localized pancreatic ductal adenocarcinoma. *PLOS Med.* **7**, e1000307 (2010).
31. T. N. Gide, C. Quek, A. M. Menzies, A. T. Tasker, P. Shang, J. Holst, J. Madore, S. Y. Lim, R. Velickovic, M. Wongchenko, Y. Yan, S. Lo, M. S. Carlino, A. Guminski, R. P. M. Saw, A. Pang, H. M. McGuire, U. Palendira, J. F. Thompson, H. Rizos, I. P. da Silva, M. Batten, R. A. Scolyer, G. V. Long, J. S. Wilmott, Distinct immune cell populations define response to anti-PD-1 monotherapy and anti-PD-1/Anti-CTLA-4 combined therapy. *Cancer Cell* **35**, 238–255 (2019).
32. S. Talbot, S. L. Foster, C. J. Woolf, Neuroimmunity: Physiology and pathology. *Annu. Rev. Immunol.* **34**, 421–447 (2016).
33. M. Levite, *Nerve-Driven Immunity. Neurotransmitters and Neuropeptides in the Immune System* (Springer, 2012).
34. C. H. Schein, Repurposing approved drugs on the pathway to novel therapies. *Med. Res. Rev.* **40**, 586–605 (2019).
35. G. Shoval, R. D. Balicer, B. Feldman, M. Hoshen, G. Eger, A. Weizman, G. Zalsman, B. Stubbs, P. Golubchik, B. Gordon, A. Krivoy, Adherence to antidepressant medications is associated with reduced premature mortality in patients with cancer: A nationwide cohort study. *Depress. Anxiety* **36**, 921–929 (2019).
36. P. M. Pilowsky, *Serotonin: The Mediator That Spans Evolution* (Elsevier, 2019).
37. M. E. Hernandez, D. Martinez-Fong, M. Perez-Tapia, I. Estrada-Garcia, S. Estrada-Parra, L. Pavón, Evaluation of the effect of selective serotonin-reuptake inhibitors on lymphocyte subsets in patients with a major depressive disorder. *Eur. Neuropsychopharmacol.* **20**, 88–95 (2010).
38. G. J. McGinnis, J. Raber, CNS side effects of immune checkpoint inhibitors: Preclinical models, genetics and multimodality therapy. *Immunotherapy* **9**, 929–941 (2017).
39. A. H. Miller, C. L. Raison, The role of inflammation in depression: From evolutionary imperative to modern treatment target. *Nat. Rev. Immunol.* **16**, 22–34 (2016).
40. D. M. Pardoll, The blockade of immune checkpoints in cancer immunotherapy. *Nat. Rev. Cancer* **12**, 252–264 (2012).
41. Y. C. Lin, Y. T. Chang, M. Campbell, T. P. Lin, C. C. Pan, H. C. Lee, J. C. Shih, P. C. Chang, MAOA-a novel decision maker of apoptosis and autophagy in hormone refractory neuroendocrine prostate cancer cells. *Sci. Rep.* **7**, 46338 (2017).
42. S. Gaur, M. E. Gross, C. P. Liao, B. Qian, J. C. Shih, Effect of Monoamine oxidase A (MAOA) inhibitors on androgen-sensitive and castration-resistant prostate cancer cells. *Prostate* **79**, 667–677 (2019).
43. Y. Liu, L. Xiao, K. I. Joo, B. Hu, J. Fang, P. Wang, In situ modulation of dendritic cells by injectable thermosensitive hydrogels for cancer vaccines in mice. *Biomacromolecules* **15**, 3836–3845 (2014).
44. B. Homet Moreno, J. M. Zaretsky, A. Garcia-Diaz, J. Tsoi, G. Parisi, L. Robert, K. Meeth, A. Ndoye, M. Bosenberg, A. T. Weeraratna, T. G. Graeber, B. Comin-Anduix, S. Hu-Lieskovan, A. Ribas, Response to programmed cell death-1 blockade in a murine melanoma syngeneic model requires costimulation, CD4, and CD8 T cells. *Cancer Immunol. Res.* **4**, 845–857 (2016).

45. S. Di Biase, X. Ma, X. Wang, J. Yu, Y.-C. Wang, D. J. Smith, Y. Zhou, Z. Li, Y. J. Kim, N. Clarke, A. To, L. Yang, Creatine uptake regulates CD8 T cell antitumor immunity. *J. Exp. Med.* **216**, 2869–2882 (2019).
46. D. J. Smith, S. Liu, S. Ji, B. Li, J. McLaughlin, D. Cheng, O. N. Witte, L. Yang, Genetic engineering of hematopoietic stem cells to generate invariant natural killer T cells. *Proc. Natl. Acad. Sci. U.S.A.* **112**, 1523–1528 (2015).
47. B. Li, X. Wang, I. Y. Choi, Y.-C. Wang, S. Liu, A. T. Pham, H. Moon, D. J. Smith, D. S. Rao, M. P. Boldin, L. Yang, miR-146a modulates autoreactive Th17 cell differentiation and regulates organ-specific autoimmunity. *J. Clin. Invest.* **127**, 3702–3716 (2017).
48. D. J. Smith, L. J. Lin, H. Moon, A. T. Pham, X. Wang, S. Liu, S. Ji, V. Rezek, S. Shimizu, M. Ruiz, J. Lam, D. M. Janzen, S. Memarzadeh, D. B. Kohn, J. A. Zack, S. G. Kitchen, D. S. An, L. Yang, Propagating humanized BLT mice for the study of human immunology and immunotherapy. *Stem Cells Dev.* **25**, 1863–1873 (2016).
49. J. Thomas, R. Khanam, D. Vohora, A validated HPLC-UV method and optimization of sample preparation technique for norepinephrine and serotonin in mouse brain. *Pharm. Biol.* **53**, 1539–1544 (2015).
50. T. M. Alshammari, A. A. Al-Hassan, T. B. Hadda, M. Aljofan, Comparison of different serum sample extraction methods and their suitability for mass spectrometry analysis. *Saudi Pharm J.* **23**, 689–697 (2015).
51. M. B. Dong, G. Wang, R. D. Chow, L. Ye, L. Zhu, X. Dai, J. J. Park, H. R. Kim, Y. Errami, C. D. Guzman, X. Zhou, K. Y. Chen, P. A. Renauer, Y. Du, J. Shen, S. Z. Lam, J. J. Zhou, D. R. Lannin, R. S. Herbst, S. Chen, Systematic immunotherapy target discovery using genome-scale in vivo CRISPR screens in CD8 T cells. *Cell* **178**, 1189–1204 (2019).

Acknowledgments: We thank the UCLA animal facility for providing animal support, the UCLA/CFAR Virology Core Laboratory for providing human PBMCs, the UCLA TCGB facility for assisting with scRNA-seq, the laboratory of M. Bosenberg (Yale University, CT, USA) for providing the MC38 cell line, the laboratory of P. Wang (University of Southern California, CA, USA) for providing the B16-OVA and PG13 cell lines, J. Mac from the laboratory of P. Wang for assisting with HPLC, and Life Science Editors for editing the manuscript. **Funding:** This work was supported by a Research Career Development Award from the STOP CANCER Foundation (to L.Y.), a BSCRC-RHF Research Award from the Rose Hills Research Foundation (to L.Y.), a JCCC/BSCRC Ablon Scholars Award from UCLA (to L.Y.), and a Magnolia Council Senior Investigator Grant Award from the Tower Cancer Research Foundation (to L.Y.). Z.L. was a postdoctoral fellow supported by the UCLA Tumor Immunology Training Grant (USHHS Ruth L. Kirschstein Institutional National Research Service award no. T32 CA009120). J.Y. was a predoctoral fellow supported by the UCLA Broad Stem Cell Research Center (BSCRC) Predoctoral Fellowship. S.Z was a predoctoral fellow supported by the UCLA Medical Scientist Training Program Grant (T32-GM008042). D.J.S was a predoctoral fellow supported by the UCLA Tumor Immunology Training Grant (U.S. Department of Health and Human Services Ruth L. Kirschstein Institutional National Research Service award no. T32 CA009056). Y-R.L. was a predoctoral fellow supported by the UCLA Whitcome Predoctoral Fellowship in Molecular Biology. **Author contributions:** X.W. and L.Y. designed the study, analyzed the data, and wrote the manuscript. X.W. performed all experiments, with the assistance from B.L. (Fig. 2C and fig. S4); Y.J.K. (Fig. 4, N and O, and fig. S8, K and M); Y.-C.W. (Fig. 1, E to H, and fig. S1B); Z.L. (Fig. 5, B and C, and figs. S1A; S11, C and D; and S12, E and F); J.Y. (Fig. 6, C and D, and fig. S12, A to D); S.Z. (Figs. 3, F and G, and 4, F to K); X.M., Y.Z., and Y.-R.L. (Fig. 1, E to H); I.Y.C., S.D.B., and D.J.S. (Fig. 2, D to F); M.P. and F.M. (Fig. 1, K to M, and figs. S2, B to F; and S3); and J.H., N.C., A.T., L.G., A.T.P., and H.M. (fig. S5A). L.Y. supervised the entire study. **Competing interests:** X.W. and L.Y. are inventors on patents related to this study filed by UCLA. The authors declare that they have no other competing interests. **Data and materials availability:** All sequencing datasets are deposited in the Genome Expression Omnibus (GEO) under accession number GSE153615. All other data supporting the findings of this study are available within the paper or in the Supplementary Materials. New viral constructs and cell lines generated in this study are available upon signing a material transfer agreement with UCLA.

Submitted 24 February 2021
Accepted 15 April 2021
Published 14 May 2021
10.1126/sciimmunol.abh2383

Citation: X. Wang, B. Li, Y. J. Kim, Y.-C. Wang, Z. Li, J. Yu, S. Zeng, X. Ma, I. Y. Choi, S. Di Biase, D. J. Smith, Y. Zhou, Y.-R. Li, F. Ma, J. Huang, N. Clarke, A. To, L. Gong, A. T. Pham, H. Moon, M. Pellegrini, L. Yang, Targeting monoamine oxidase A for T cell–based cancer immunotherapy. *Sci. Immunol.* **6**, eabh2383 (2021).

Science Immunology

Targeting monoamine oxidase A for T cell–based cancer immunotherapy

Xi Wang, Bo Li, Yu Jeong Kim, Yu-Chen Wang, Zhe Li, Jiaji Yu, Samuel Zeng, Xiaoya Ma, In Young Choi, Stefano Di Biase, Drake J. Smith, Yang Zhou, Yan-Ruide Li, Feiyang Ma, Jie Huang, Nicole Clarke, Angela To, Laura Gong, Alexander T. Pham, Heesung Moon, Matteo Pellegrini and Lili Yang

Sci. Immunol. **6**, eabh2383.
DOI: 10.1126/sciimmunol.abh2383

Repurposing antidepressants for cancer immunotherapy

Antibodies targeting immune checkpoints that restrain the antitumor effects of T cells are now a proven therapeutic approach for many forms of human cancer. The search for additional drug-targetable checkpoint molecules that regulate tumor immunity continues. Wang *et al.* identified monoamine oxidase A (MAO-A) as a gene up-regulated in tumor-infiltrating immune cells in mice. Tumor cells grew at a slower rate in mutant mice with decreased MAO-A expression. Inhibition of MAO-A activity by the antidepressant drug phenelzine enhanced the resistance of wild-type mice to tumor growth and exhibited synergy with anti –PD-1 treatment. These findings set the stage for further studies assessing the potential of repurposed MAO-A inhibitor drugs in the immunotherapy of cancer.

Science Immunology
AAAS

immunology.sciencemag.org/cgi/content/full/6/59/eabh2383/DC1

Supplementary Materials for

Targeting monoamine oxidase A for T cell–based cancer immunotherapy

Xi Wang, Bo Li, Yu Jeong Kim, Yu-Chen Wang, Zhe Li, Jiaji Yu, Samuel Zeng, Xiaoya Ma, In Young Choi, Stefano Di Biase, Drake J. Smith, Yang Zhou, Yan-Ruide Li, Feiyang Ma, Jie Huang, Nicole Clarke, Angela To, Laura Gong, Alexander T. Pham, Heesung Moon, Matteo Pellegrini, Lili Yang*

*Corresponding author. Email: liliyang@ucla.edu

Published 14 May 2021, *Sci. Immunol.* **6**, eabh2383 (2021)
DOI: 10.1126/sciimmunol.abh2383

The PDF file includes:

Other Supplementary Material for this manuscript includes the following:

(available at immunology.sciencemag.org/cgi/content/full/6/59/eabh2383/DC1)

Table S2. Raw data file (Excel spreadsheet).
Reproducibility checklist (Microsoft Excel format).

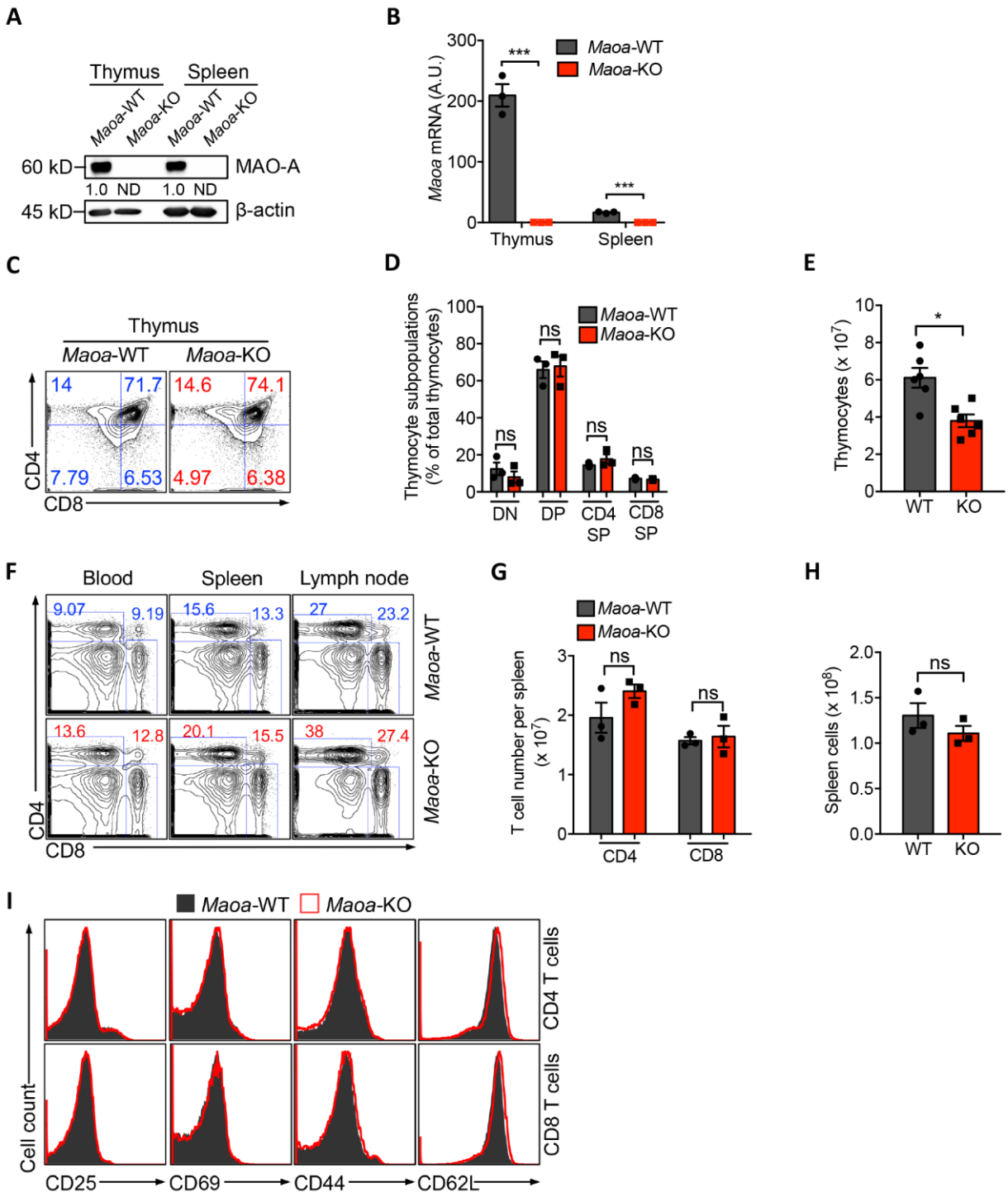

Fig. S1. Characterization of *Maoa*-KO mice (related to Fig. 1).

(**A** and **B**) MAO-A expression in the lymphoid organs of *Maoa*-WT and *Maoa*-KO mice (n = 3). (A) Western blot analyses of MAO-A protein expression. (B) qPCR analyses of *Maoa* mRNA expression. ND, nondetectable.

(**C** to **E**) T cell development in the thymi of *Maoa*-WT and *Maoa*-KO mice (n = 3). (C) FACS

plots showing the developmental stages of thymocytes defined by CD4/CD8 co-receptor expression. DN, double-negative; DP, double-positive; CD4 SP, CD4 single-positive; CD8 SP, CD8 single-positive. (D) Quantification of C. (E) Numbers of total thymocytes.
(**F** to **H**) T cell presence in the periphery of *Maoa*-WT and *Maoa*-KO mice (n = 3). (F) FACS plots showing the detection of CD4 and CD8 T cells (gated as $TCR\beta^{+}CD4^{+}$ and $TCR\beta^{+}CD8^{+}$ cells, respectively) in the peripheral blood, spleen, and lymph nodes. (G) Quantification of F. (H) Numbers of total splenocytes.
(**I**) T cell phenotype in the spleen of *Maoa*-WT and *Maoa*-KO mice prior to tumor challenge (n = 3). Representative FACS plots are presented, showing a typical naïve phenotype ($CD25^{lo}CD69^{lo}CD44^{lo}CD62L^{hi}$) of T cells in both mice.
Representative of two experiments. Data are presented as the mean ± SEM. ns, not significant, ***$P < 0.001$, by Student's *t* test.

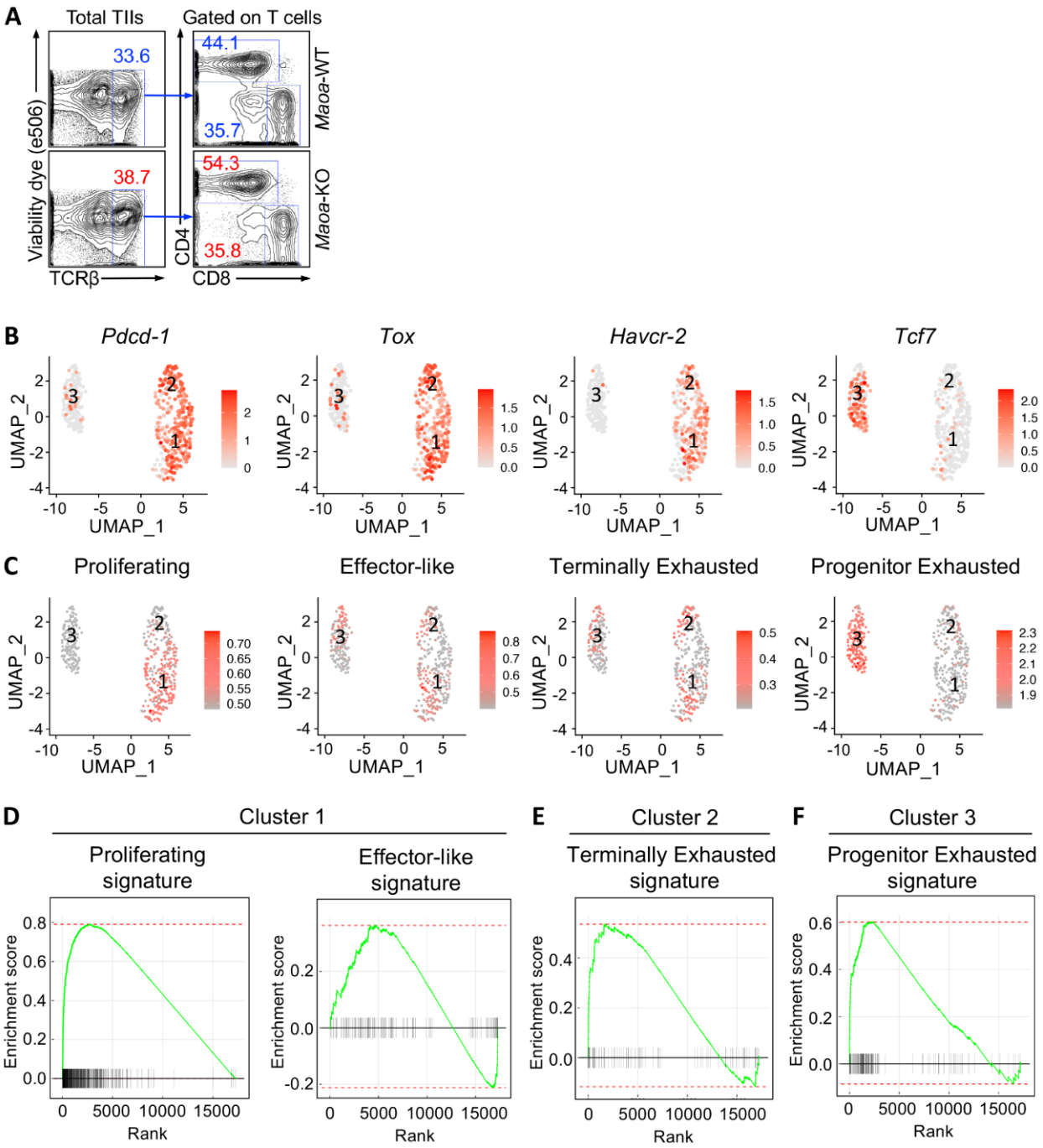

Fig. S2. MAO-A–deficient mice show suppressed tumor growth and enhanced CD8 T cell antitumor immunity (related to Fig. 1, E to M).

(**A**) T cell tumor infiltration in day 14 B16-OVA tumors grown in *Maoa*-WT and *Maoa*-KO mice (n = 5). Representative FACS plots are presented, showing the detection of comparable levels of tumor-infiltrating immune cells (TIIs; pre-gated as $CD45.2^+$ cells) comprising CD4 and CD8 T cells (gated as $TCR\beta^+CD4^+$ and $TCR\beta^+$ $CD8^+$ cells, respectively).

(**B to F**) scRNA-seq analysis of antigen-experienced ($CD44^+$) tumor-infiltrating CD8 T cells isolated from day 14 B16-OVA tumors grown in *Maoa*-WT and *Maoa*-KO mice (10 tumors

were combined for each group). (B) UMAP plots showing the expression of indicated signature genes in individual cells. Each dot represents an individual cell and is colored according to its expression level of the indicated gene; the three cell clusters are marked. (C) UMAP plots showing the expression of a signature of genes upregulated in proliferating, effector-like, terminally exhausted, or progenitor exhausted CD8 T cells (GSE122713) in individual cells. Each dot represents an individual cell and is colored according to the combined expression of the indicated signature of genes; the three cell clusters are marked. (D to F) Gene Set Enrichment Analysis (GSEA) plots showing the enrichment of indicated gene signatures (GSE122713) in cluster 1 cells (proliferating and effector-like CD8 T cell gene signatures; D), cluster 2 cells (terminally exhausted CD8 T cell gene signature; E), and cluster 3 cells (progenitor exhausted CD8 T cell gene signature; F).
Representative of one (B to F) and three (A) experiments.

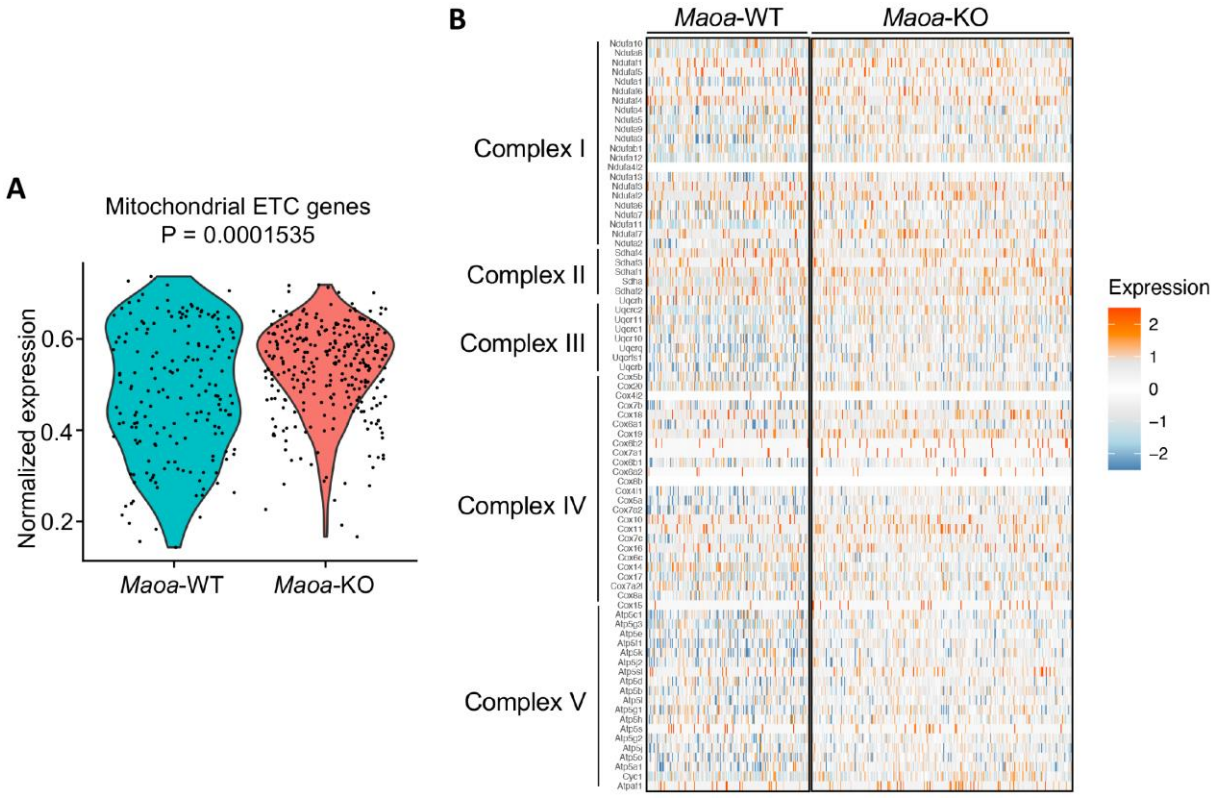

Fig. S3. MAO-A–deficient tumor-infiltrating CD8 T cells show enhanced mitochondrial electron transport chain (ETC) gene expression (related to Fig. 1, K to M).

scRNA-seq analysis of antigen-experienced ($CD44^+$) tumor-infiltrating CD8 T cells isolated from day 14 B16-OVA tumors grown in *Maoa*-WT and *Maoa*-KO mice (10 tumors were combined for each group), showing the enhanced expression of mitochondrial ETC genes in *Maoa*-KO CD8 T cells compared to that in *Maoa*-WT CD8 T cells. A total of 80 genes encoding the mitochondrial ETC complexes I to V were studied.

(**A**) Violin plots showing the expression distribution of mitochondrial ETC genes. Each dot represents an individual cell, and its combined expression of all 80 ETC genes is presented.

(**B**) Heatmaps showing the expression of individual mitochondrial ETC genes. Each column indicates a single cell. Each row indicates an individual ETC gene.

Representative of one experiment. *P* value of the violin plot (A) was determined by Wilcoxon rank sum test.

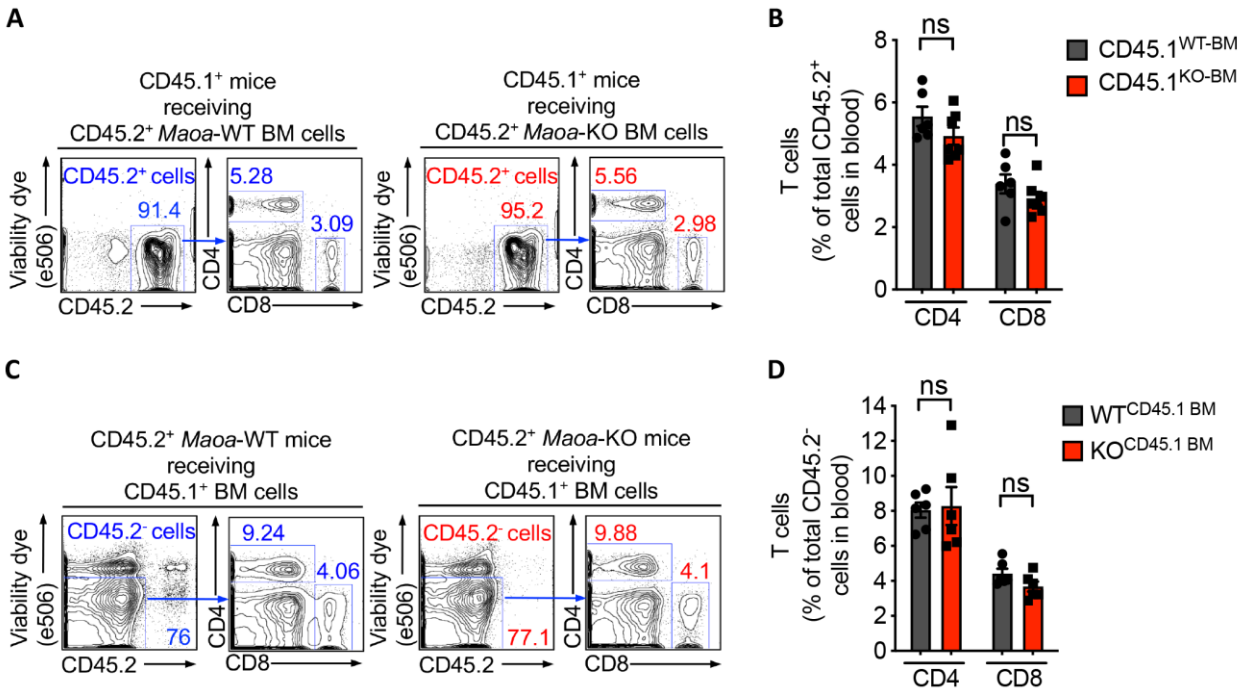

Fig. S4. MAO-A directly regulates antitumor immunity (related to Fig. 2, A to C).
(**A** and **B**) T cell reconstitution in CD45.1 wildtype recipient mice receiving bone marrow (BM) cells from the *Maoa*-WT or *Maoa*-KO donor mice (denoted as $CD45.1^{WT\text{-}BM}$ or $CD45.1^{KO\text{-}BM}$ mice, respectively; n = 6-7). (A) FACS plots showing the detection of comparable levels of CD4 and CD8 T cells (gated as $CD45.2^{+}CD4^{+}$ and $CD45.2^{+}CD8^{+}$ cells, respectively) in the blood of $CD45.1^{WT\text{-}BM}$ or $CD45.1^{KO\text{-}BM}$ mice. (B) Quantification of A.
(**C** and **D**) T cell reconstitution in *Maoa*-WT and *Maoa*-KO recipient mice receiving bone marrow cells from CD45.1 wildtype donor mice (denoted as $WT^{CD45.1\ BM}$ or $KO^{CD45.1\ BM}$ mice, respectively; n = 6). (C) FACS plots showing the detection of comparable levels of CD4 and CD8 T cells (gated as $CD45.2^{-}CD4^{+}$ and $CD45.2^{-}CD8^{+}$ cells, respectively) in the blood of $WT^{CD45.1\ BM}$ or $KO^{CD45.1\ BM}$ mice. (D) Quantification of C.
Representative of two experiments. Data are presented as the mean ± SEM. ns, not significant, by Student's *t* test.

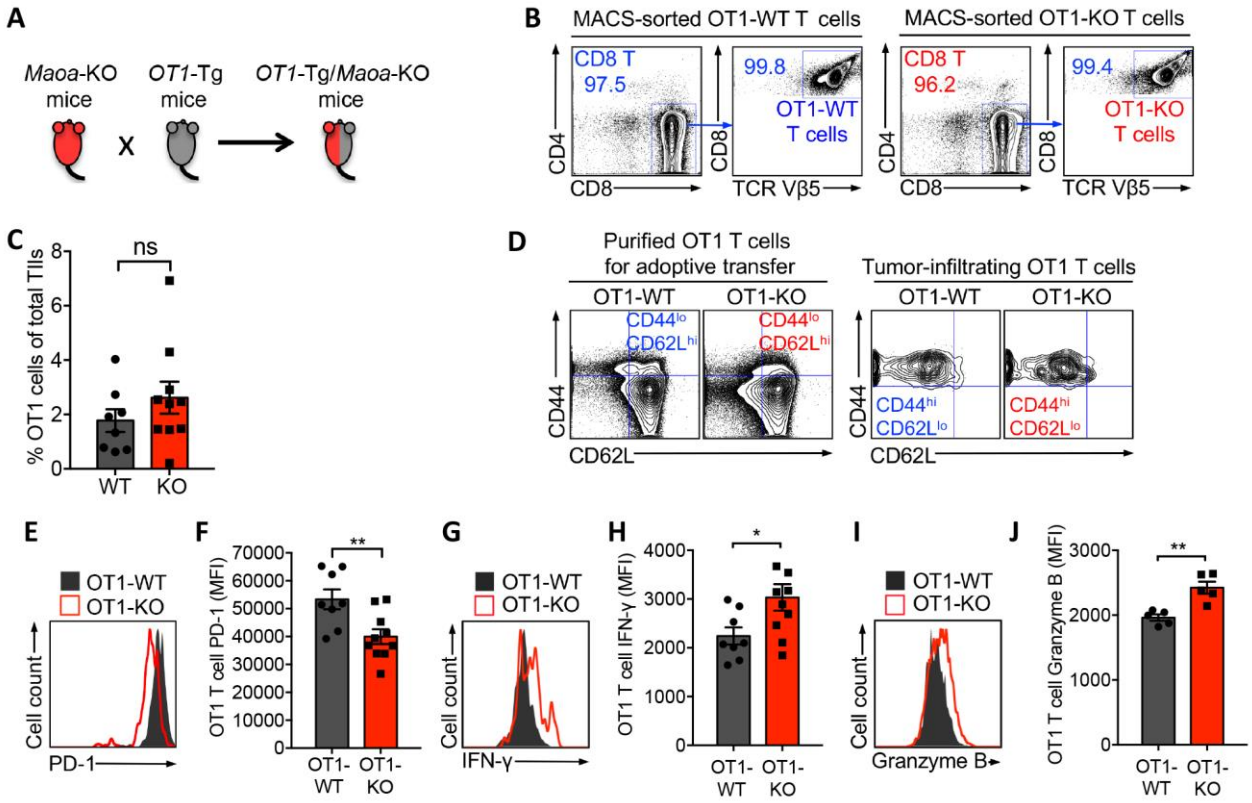

Fig. S5. MAO-A directly regulates CD8 T cell antitumor immunity (related to Fig. 2, D to F).

(**A**) Breeding strategy for the generation of *OT1* transgenic (*OT1*-Tg) mice deficient of *Maoa* gene (denoted as the *OT1*-Tg/*Maoa-KO* mice).

(**B**) FACS plots showing the isolation of high-purity OT1 transgenic T cells (> 99% purity; gated as $CD4^{-}CD8^{+}TCR\ V\beta5^{+}$ cells) from the *OT1*-Tg and *OT1*-Tg/*Maoa*-KO mice (denoted as OT1-WT and OT1-KO T cells, respectively).

(**C** to **J**) Antitumor reactivity of OT1-WT and OT1-KO T cells adoptively transferred into CD45.1 wildtype mice bearing B16-OVA tumors (n = 5-10). The experimental design is shown in Fig. 2D. Tumors were collected from experimental mice on day 17 post tumor inoculation, followed by TII isolation and FACS analysis. (C) FACS quantification of tumor-infiltrating OT1-WT and OT1-KO T cells (gated as $CD45.2^{+}CD8^{+}$ cells). (D) FACS plots showing the antigen-experienced phenotype ($CD44^{hi}CD62L^{lo}$) of tumor-infiltrating OT1-WT and OT1-KO T cells. Note prior to adoptive transfer, both the purified OT1-WT and OT1-KO T cells displayed a naïve T cell phenotype ($CD44^{lo}CD62^{hi}$). (E and F) FACS plots and quantifications showing the PD-1 expression on tumor-infiltrating OT1-WT and OT1-KO T cells. (G and H) FACS plots and quantifications showing the measurements of intracellular cytokine (IFN-γ) production by tumor-infiltrating OT1-WT and OT1-KO T cells. (I and J) FACS plots and quantifications showing the measurements of intracellular cytotoxic molecule (i.e., Granzyme B) production by tumor-infiltrating OT1-WT and OT1-KO T cells.

Representative of two experiments. Data are presented as the mean ± SEM. ns, not significant; $*P < 0.05$, $**P < 0.01$, by Student's *t* test.

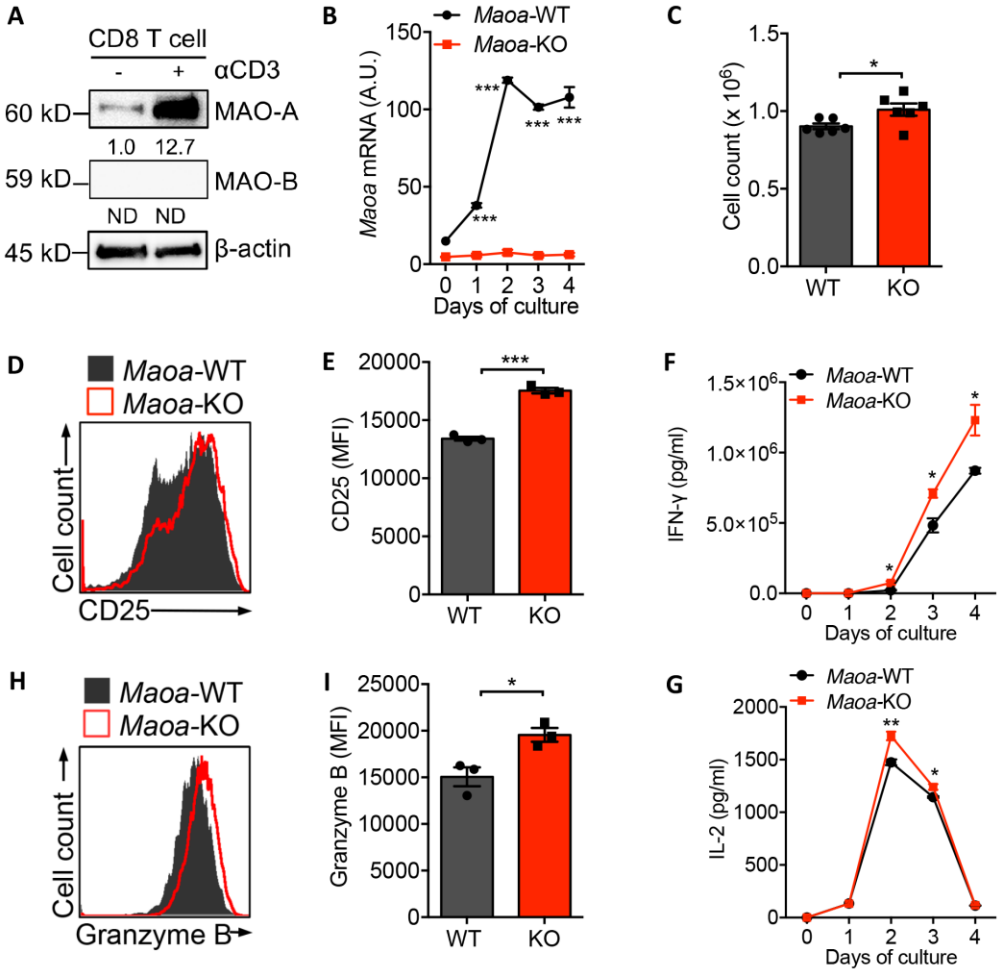

Fig. S6. MAO-A acts as a negative-feedback regulator to restrain CD8 T cell activation (related to Fig. 3).

(**A**) Western blots showing the detection of MAO-A and MAO-B proteins in CD8 T cells. CD8 T cells were purified from the spleen and lymph nodes of *Maoa*-WT mice, stimulated *in vitro* with anti-CD3 for 2 days, followed by total protein extraction and Western blot analysis.

(**B** to **I**) Studying CD8 T cell activation *in vitro* with anti-CD3 and anti-CD28 co-stimulation (n = 3). CD8 T cells were purified from *Maoa*-WT and *Maoa*-KO mice and stimulated *in vitro* with anti-CD3 and anti-CD28. The analyses of *Maoa* mRNA expression (B), cell proliferation (C), activation marker expression (i.e., CD25; D and E), effector cytokine production (i.e., IL-2 and IFN-γ; F and G), and cytotoxic molecule production (i.e., Granzyme B; H and I) are presented, either over a 4-day time course (B, F, and G), or on day 3 after stimulation (C to E, H and I).

Representative of two experiments. Data are presented as the mean ± SEM. **P* < 0.05, ***P* < 0.01, ****P* < 0.001, by Student's *t* test.

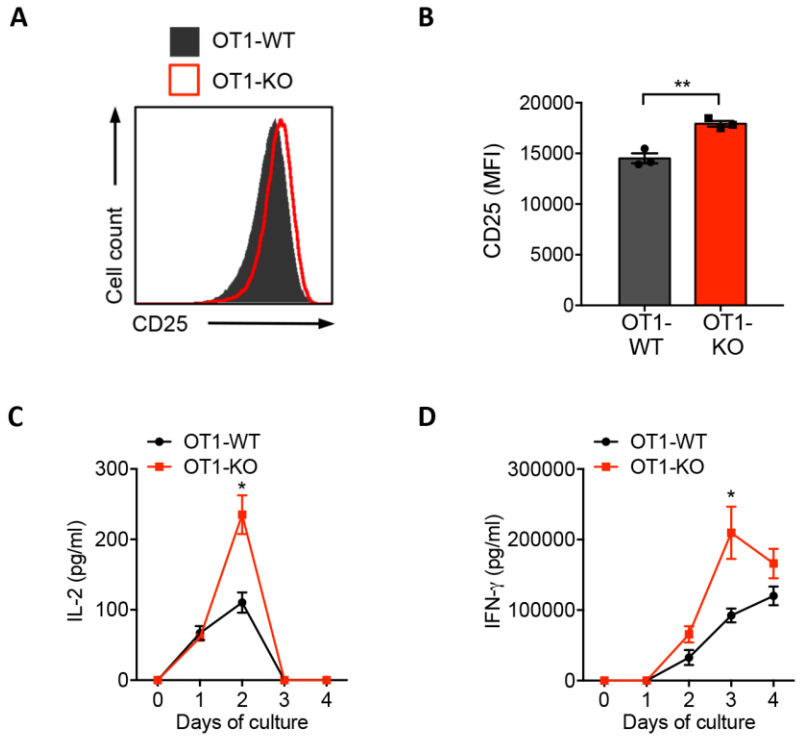

Fig. S7. MAO-A acts as a negative-feedback regulator to restrain CD8 T cell activation: Studying antigen-specific T cells (related to Fig. 3).

OVA-specific OT1 transgenic CD8 T cells were isolated from the *OT1*-Tg or *OT1*-Tg/*Maoa*-KO mice (denoted as OT1-WT or OT1-KO T cells, respectively), then stimulated *in vitro* with anti-CD3 (n = 3).

(**A**) FACS plot showing the CD25 expression on OT1-WT and OT1-KO T cells at day 3 after anti-CD3 stimulation.

(**B**) Quantification of A.

(**C** and **D**) ELISA analyses of IL-2 (C) and IFN-γ (D) production by OT1-WT and OT1-KO T cells over a 4-day time course after anti-CD3 stimulation.

Representative of three experiments. Data are presented as the mean ± SEM. **P* < 0.05, ***P* < 0.01, by Student's *t* test.

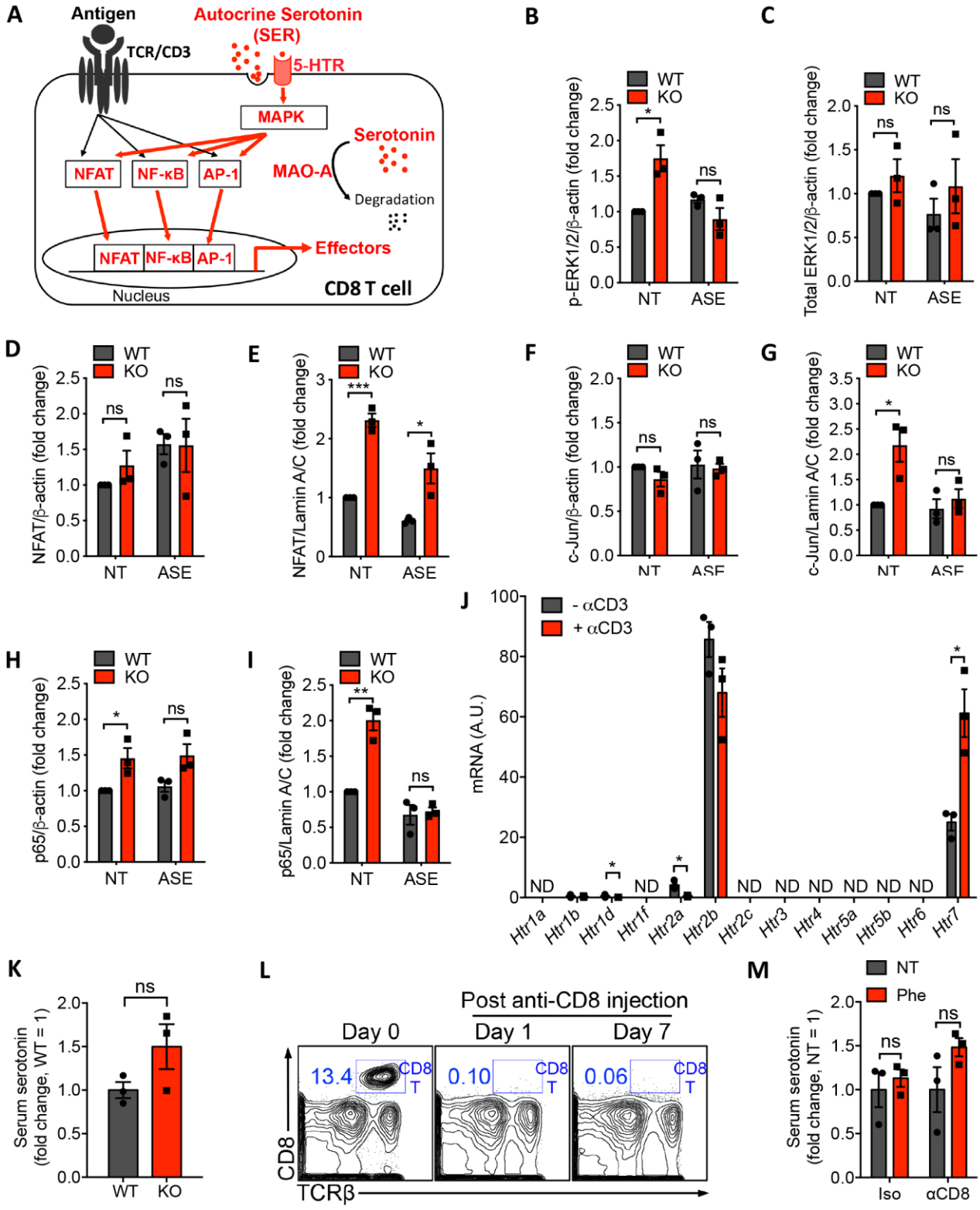

Fig. S8. MAO-A regulates CD8 T cell autocrine serotonin signaling (related to Fig. 4).
(**A**) Schematic model showing the cross-talk between 5-HTR and TCR signaling pathways in a

CD8 T cell. Experimentally confirmed signaling molecules and pathways are highlighted in red.
(**B to I**) CD8 T cell 5-HTR and TCR signaling cross-talk *in vitro*. Quantification of Western blots shown in main text Fig. 4, L and M. *Maoa*-WT and *Maoa*-KO CD8 T cells were stimulated with anti-CD3 for 2 days, in the presence or absence of asenapine (ASE). Cells were then rested on ice for 2 hours and restimulated with anti-CD3 for 20 minutes, followed by total protein extraction (B and C), or nuclear protein extraction and cytoplasmic protein extraction (NE and CE; D to I), and Western blot analysis of key signaling molecules involved in 5-HTR (B and C) and TCR (D to I) signaling pathways (n = 3). (B and C) Quantification of Western blots shown in main text Fig. 4L. (D to I) Quantification of Western blots shown in main text Fig. 4M.
(**J**) qPCR analyses of 5-HTR family member mRNA expression in CD8 T cells. CD8 T cells were purified from B6 wildtype mice and stimulated with anti-CD3 for 24 hours (n = 3).
(**K** to **M**) CD8 T cell serotonin production *in vivo* in a B16-OVA melanoma model (n = 3). On day 14 after tumor challenge, sera were collected from experimental mice for serotonin measurement using HPLC. (K) Serum serotonin levels in *Maoa*-WT and *Maoa*-KO mice (denoted as WT and KO, respectively). (L) Representative FACS plots showing the successful *in vivo* depletion of CD8 T cells induced by anti-CD8 antibody injection. (M) Serum serotonin levels in *Maoa*-WT mice, with or without phenelzine treatment (Phe or NT), and with or without antibody-induced depletion of CD8 T cells (aCD8 or Iso).
Representative of two (K to M) and three (B to J) experiments. Data are presented as the mean ± SEM. ns, not significant, $*P < 0.05$, $**P < 0.01$, by Student's *t* test.

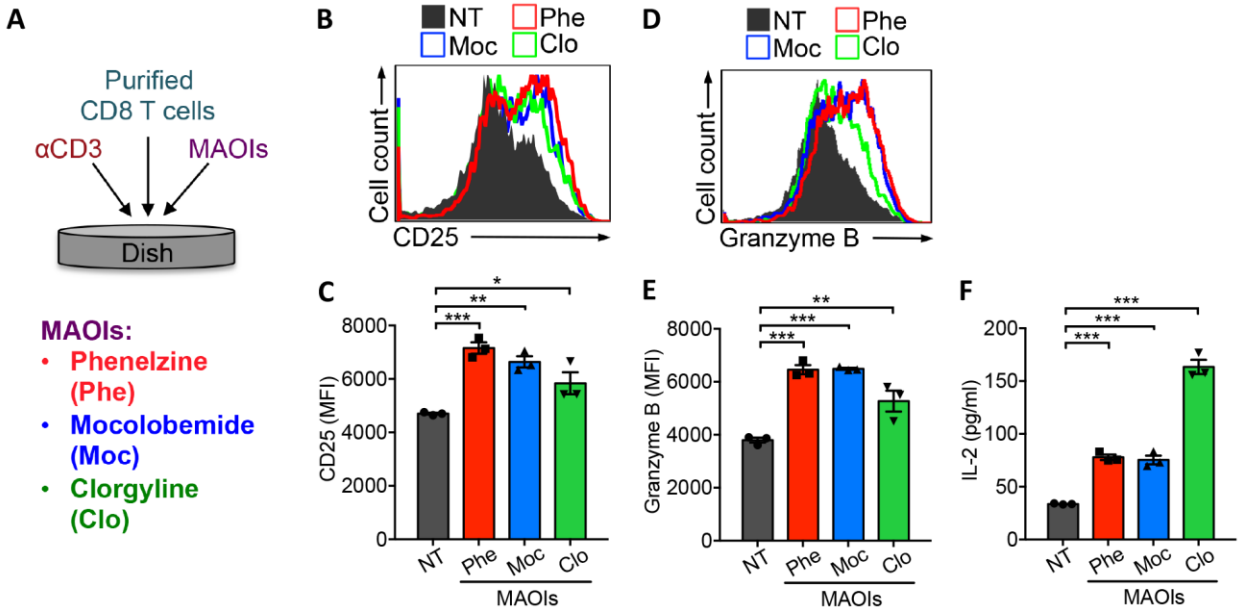

Fig. S9. MAOI treatment induces CD8 T cell hyperactivation in vitro (related to Fig. 5A).
(**A**) Experimental design. CD8 T cells were purified from B6 wildtype mice and stimulated with anti-CD3 *in vitro*, in the absence (NT) or presence of MAOIs (phenelzine, Phe; moclobemide, Moc; and clorgyline, Clo). N = 3.
(**B**) FACS plots showing the measurement of cell surface CD25 expression on day 2 after anti-CD3 stimulation.
(**C**) Quantification of (B).
(**D**) FACS plots showing the measurement of intracellular Granzyme B production on day 2 after anti-CD3 stimulation.
(**E**) Quantification of (D).
(**F**) ELISA analyses of IL-2 production on day 3 after anti-CD3 stimulation.
Representative of three experiments. Data are presented as the mean ± SEM. **P* < 0.05, ***P* < 0.01, ****P* < 0.001, by one-way ANOVA.

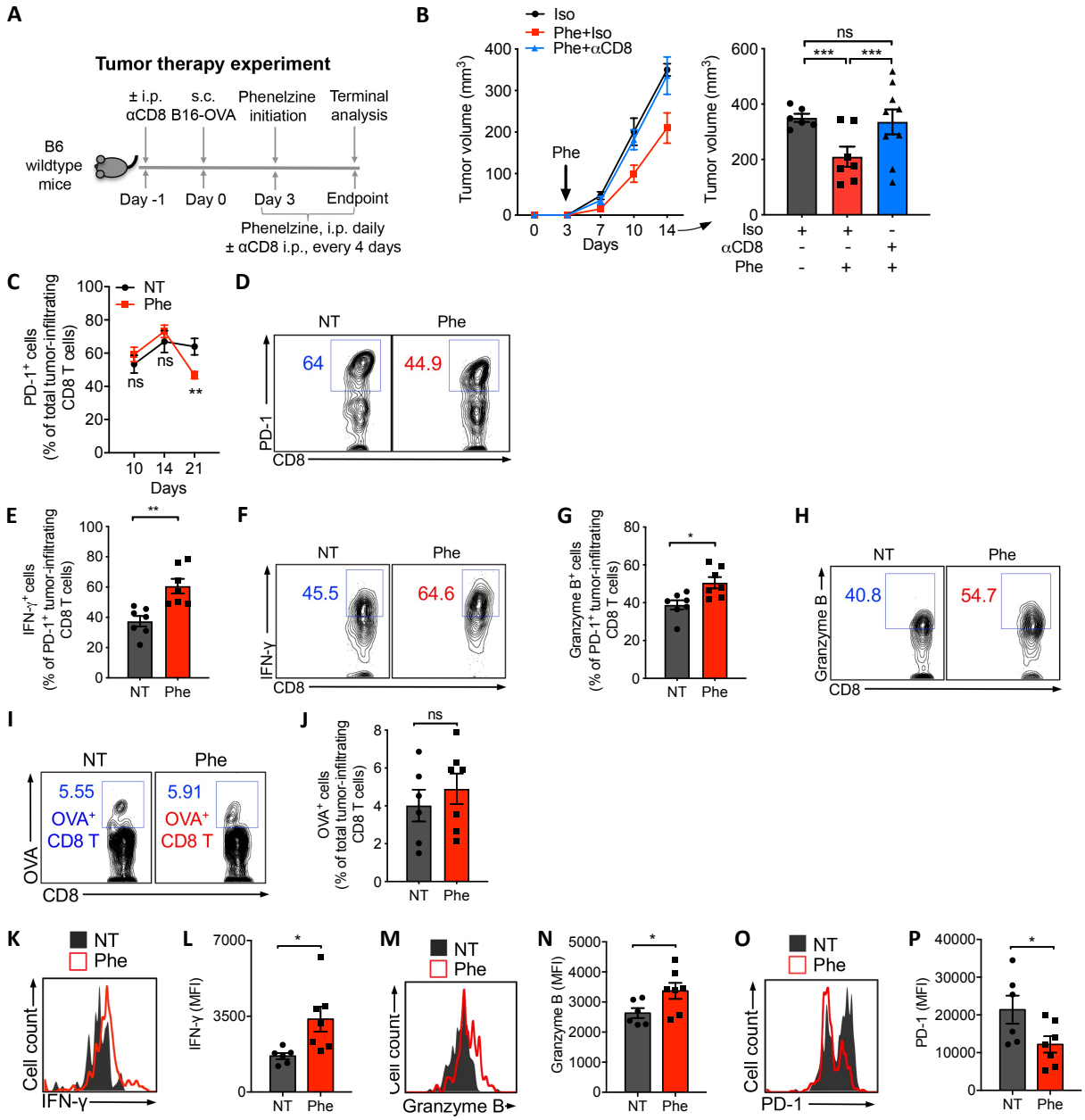

Fig. S10. MAO-A blockade for cancer immunotherapy: Syngeneic mouse tumor model studies (related to Fig. 5).

(**A** and **B**) Cancer therapy potential of MAOI treatment and its CD8 T cell-dependency in a B16-OVA melanoma model. (A) Experimental design. (B) Tumor growth in B6 wildtype mice with or without phenelzine treatment and with or without anti-CD8 treatment to deplete CD8 T cells (Iso, Phe+Iso, or Phe+αCD8; n = 6-9).

(**C** to **H**) MAO-A regulation of T cell exhaustion at different stages in a B16-OVA tumor model. B6 wildtype mice were inoculated with B16-OVA tumor cells (1×10^6 cells per animal) with or without phenelzine treatment (Phe or NT; n = 5-9). Tumor samples were collected at the indicated time points after tumor challenge and analyzed by flow cytometry. (C) FACS quantification of PD-1^+ tumor-infiltrating CD8 T cells over time. (D) FACS plots showing the detection of PD-1^+ tumor-infiltrating CD8 T cells at day 21. (E to H) Functionality analysis of PD-1^+ tumor-infiltrating CD8 T cells at day 21. FACS plots and quantifications of intracellular IFN-γ (E and F) and Granzyme B (G and H) production are presented.

(**I** to **P**) Antigen-specific CD8 T cell antitumor responses under MAOI treatment in a B16-OVA

melanoma model. B6 wildtype mice were inoculated with B16-OVA melanoma cells (1×10^6 cells per animal), with or without phenelzine treatment on day 3 post tumor inoculation (Phe or NT; n = 6-7). Tumor samples were collected on day 14 after tumor inoculation and analyzed by flow cytometry. OVA-specific CD8 T cells were gated as $CD45.2^+TCR\beta^+CD8^+OVA^+$ cells. (I and J) FACS plots and quantifications are presented showing the frequencies of OVA-specific tumor-infiltrating CD8 T cells. (K to N) FACS plots and quantifications are presented showing the measurements of intracellular IFN-γ (K and L) and Granzyme B (M and N) production. (O and P) FACS plots and quantifications are presented showing the measurements of PD-1 expression.

Representative of two experiments. Data are presented as the mean ± SEM. ns, not significant, $*P < 0.05$, $**P < 0.01$, $***P < 0.001$, by Student's *t* test.

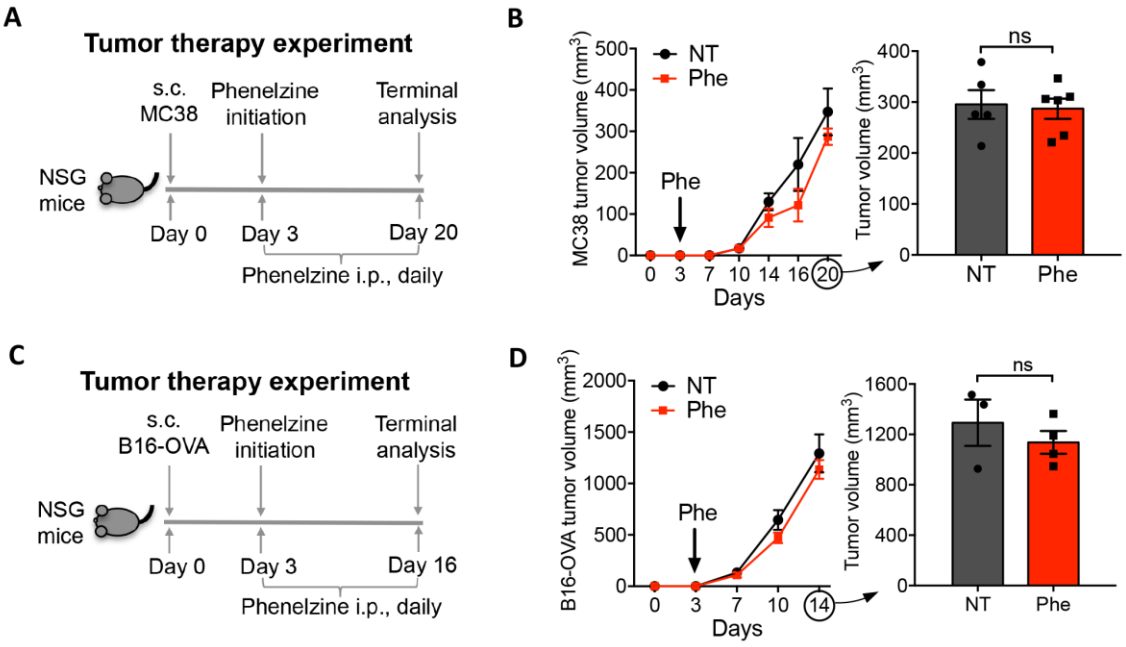

Fig. S11. MAO-A blockade for cancer immunotherapy: Immunodeficient NSG mouse tumor model studies (related to Fig. 5).

(**A** and **B**) Studying MC38 tumor growth in immunodeficient NSG mice with or without phenelzine treatment (Phe or NT). (A) Experimental design. (B) Tumor growth (n = 5-6).

(**C** and **D**) Studying B16-OVA tumor growth in NSG mice with or without phenelzine treatment (Phe or NT). (C) Experimental design. (D) Tumor growth (n = 3-4).

Representative of two experiments. Data are presented as the mean ± SEM. ns, not significant, by Student's *t* test.

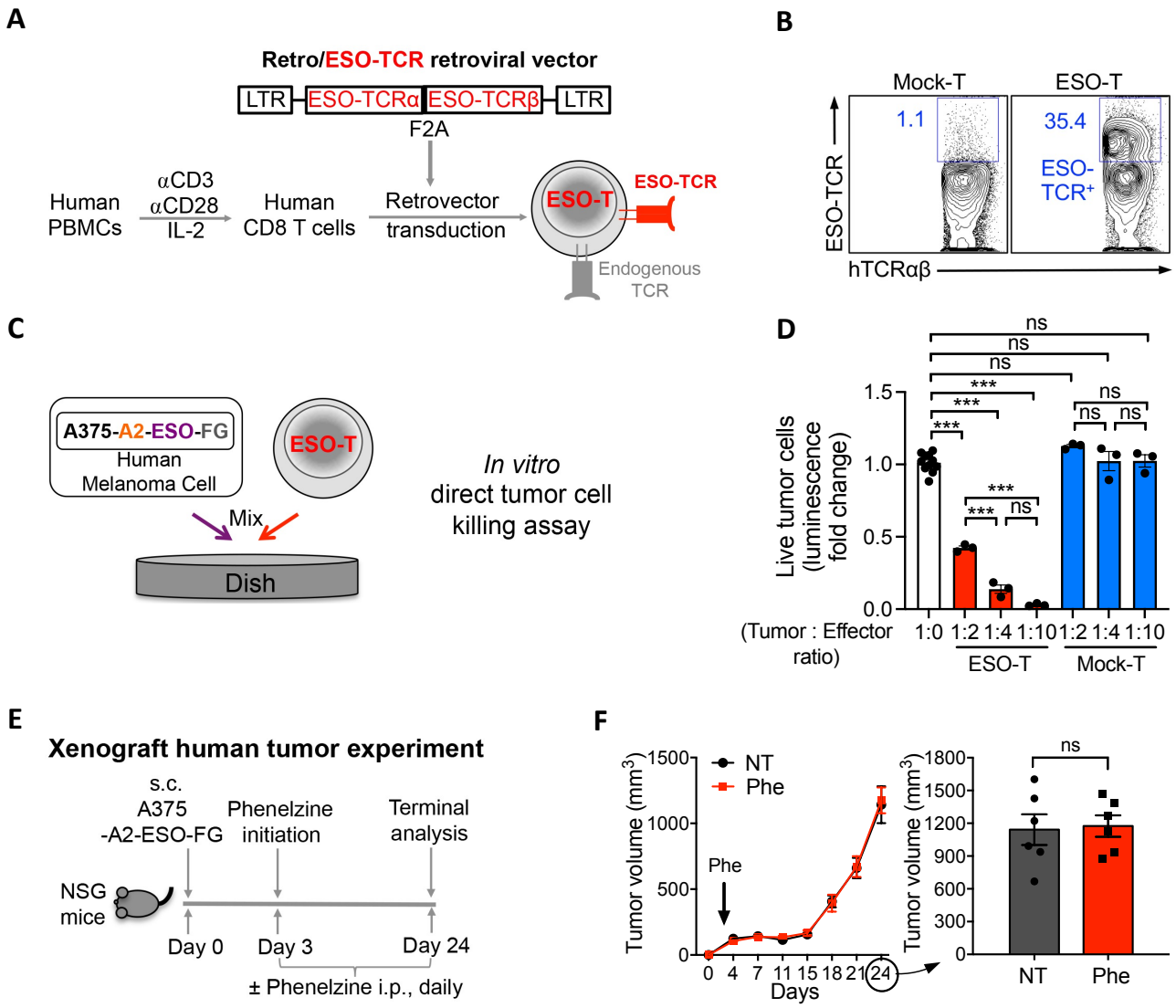

Fig. S12. MAO-A blockade for cancer immunotherapy: Human T cell studies (related to Fig. 6, A to D).

(**A**) Schematics showing the strategy to generate human CD8 T cells recognizing the NY-ESO-1 tumor antigen. Healthy donor peripheral blood mononuclear cells (PBMCs) were stimulated *in vitro* with anti-CD3/CD28 and IL-2 to expand human CD8 T cells, followed by transduction with a Retro/ESO-TCR retrovector encoding an HLA-A2-restricted NY-ESO-1 specific TCR (clone 3A1). The resulting human CD8 T cells, denoted as the ESO-T cells, can specifically target the A375-A2-ESO-FG human melanoma cells.

(**B**) FACS plots showing the detection of ESO-TCR expression on the engineered ESO-T cells. Human CD8 T cells that received mock transduction were included as a staining control (denoted as Mock-T cells).

(**C**) Experimental design to study the *in vitro* direct killing of A375-A2-ESO-FG human melanoma cells by ESO-T cells.

(**D**) Tumor killing data from C (n = 3-6).

(**E** and **F**) A375-A2-ESO-FG tumors growth in NSG mice with or without phenelzine treatment (Phe or NT). (E) Experimental design. (F) Tumor growth (n = 6).

Representative of two experiments. Data are presented as the mean ± SEM. ns, not significant, **P* < 0.05, ****P* < 0.001, by one-way ANOVA (D) or by Student's *t* test (F).

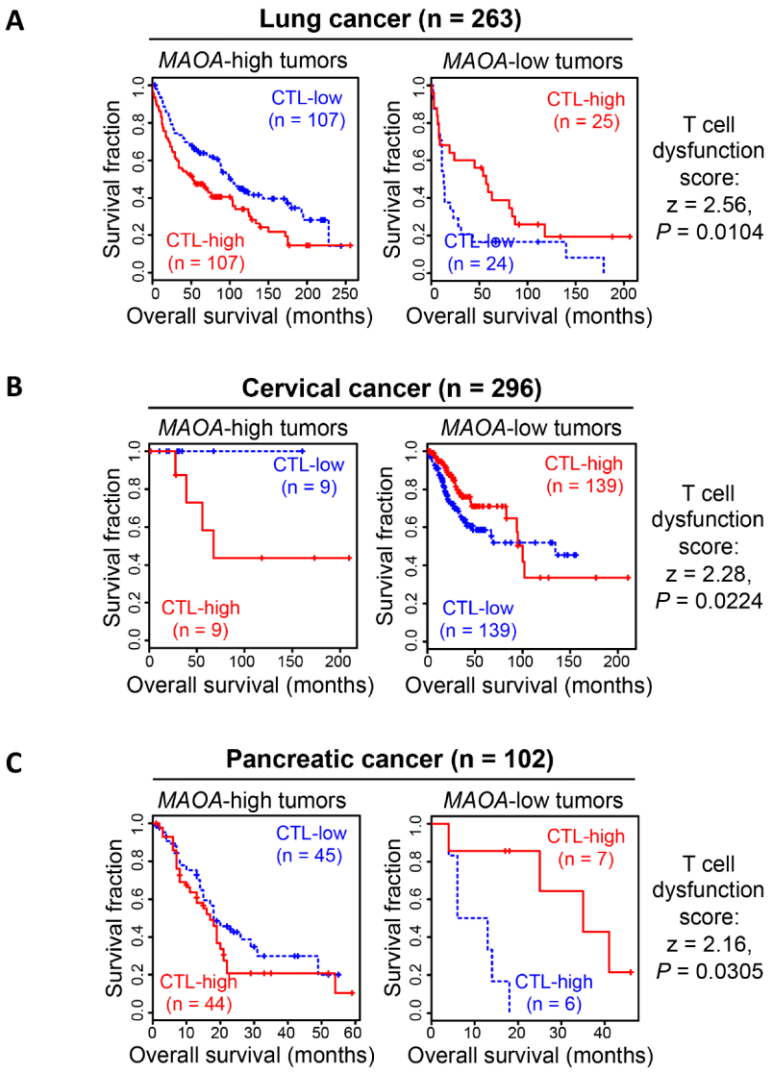

Fig. S13. Clinical data correlation studies identify MAO-A as a negative regulator of T cell antitumor function in patients with cancer (related to Fig. 6, E and F).

A Tumor Immune Dysfunction and Exclusion (TIDE) computational method was used to study the association between the tumor-infiltrating CD8 T cell (also known as cytotoxic T lymphocyte, CTL) level and overall patient survival in relation to the intratumoral *MAOA* gene expression level. For each patient cohort, tumor samples were divided into *MAOA*-high (samples with *MAOA* expression one standard deviation above the average; shown in left survival plot) and *MAOA*-low (remaining samples; shown in right survival plot) groups, followed by analyzing the association between CTL levels and survival outcomes in each group. The CTL level was estimated as the average expression level of *CD8A*, *CD8B*, *GZMA*, *GZMB*, and *PRF1*. Each survival plot presented tumors in two subgroups: "CTL-high" group (red) had above-average CTL values among all samples, while 'CTL-low' group (blue) had below-average CTL values. A T cell dysfunction score (*z* score) was calculated for each patient cohort, correlating the *MAOA* expression level with the beneficial effect of CTL infiltration on patient survival. A positive *z* score indicates that the expression of *MAOA* is negatively correlated with the beneficial effect of tumor-infiltrating CTL on patient survival. The *P* value indicates the comparison between the *MAOA*-low and *MAOA*-high groups, and was calculated by two-sided Wald test in a Cox-PH

regression.
(**A**) TIDE analysis of a lung cancer patient cohort (GSE30219; n = 263). $z = 2.56$; $P = 0.0104$.
(**B**) TIDE analysis of a cervical cancer patient cohort (TCGA; n = 296). $z = 2.28$; $P = 0.0224$.
(**C**) TIDE analysis of a pancreatic cancer patient cohort (GSE21501@PRECOG; n = 102). $z = 2.16$; $P = 0.0305$.

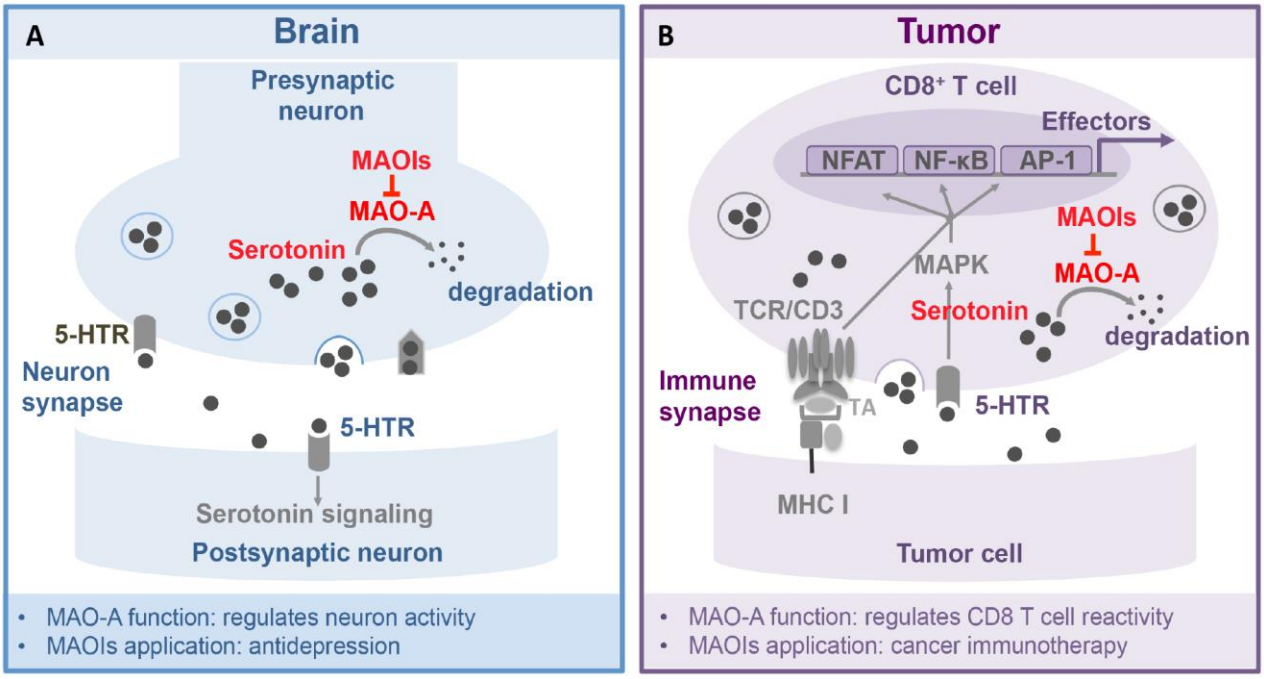

Fig. S14. The intratumoral MAO-A–serotonin axis model.
(**A**) Schematics showing the "MAO-A-serotonin axis" in the brain regulating neuron activity. A presynaptic neuron and a postsynaptic neuron form a neuron synapse. The presynaptic neuron produces serotonin, which is provided to the postsynaptic neuron for neuronal signal transmission. The presynaptic neuron also expresses MAO-A that controls serotonin degradation thereby regulating neuron activity. MAOIs have been clinically used for treating depression symptoms, targeting the "MAO-A-serotonin axis" in the brain.
(**B**) Schematics showing the "MAO-A-serotonin axis" in tumors regulating CD8 T cell antitumor reactivity. Analogous to neurons in brain, a tumor-specific CD8 T cell and a tumor cell form an immune synapse. The CD8 T cell produces serotonin that enhances TCR/TA (tumor antigen) recognition-induced T cell activation. The CD8 T cell also expresses MAO-A, which controls serotonin degradation thereby regulating CD8 T cell antitumor reactivity. Established MAOI antidepressants can potentially be repurposed for enhancing T cell-based cancer immunotherapy, targeting the "MAO-A-serotonin axis" in tumors.

Table S1. Primer sequences for qPCR.

Maoa	Exon12 forward	CCTGGTATCATGACTCTGTATGG
	Exon14 reverse	CTTGGACTCAGGCTCTTGAAC
Maoa (for MIG-Maoa retrovector)	Forward	GTACCCGCTTTGGAGATAAC
	Reverse	GAAGGGCCACTGATGTGGAA
Ifng	Forward	ATGAACGCTACACACTGCATC
	Reverse	CCATCCTTTTGCCAGTTCCTC
Il2	Forward	TGAGCAGGATGGAGAATTACAGG
	Reverse	GTCCAAGTTCATCTTCTAGGCAC
Gzmb	Forward	CCTCCTGCTACTGCTGAC
	Reverse	GTCAGCACAAAGTCCTCTC
Tph1	Forward	CACGAGTGCAAGCCAAGGTTT
	Reverse	AGTTTCCAGCCCCGACATCAG
Ube2d2	Forward	ACAAGGAATTGAATGACCTGGC
	Reverse	CACCCTGATAGGGGCTGTC
MAOA	Forward	GTCTTAAATGGTCTCGGGAAGG
	Reverse	CCAGAAGGTGTGGGTGATTT
ACTIN	Forward	GAGCACAGAGCCTCGCCTTT
	Reverse	ACATGCCGGAGCCGTTGTC